https://doi.org/10.5194/nhess-2022-83
Preprint. Discussion started: 9 March 2022

Natural Hazards and Earth System Sciences
Discussions
Open Access
EGU

Earthquake-induced landslides in Haiti: seismotectonic and climatic influences, size-frequency relationships

Hans-Balder Havenith[1], Kelly Guerrier[2], Romy Schlögel[1,3], Anne-Sophie Mreyen[4], Sophia Ulysse[2,5], Anika Braun[6], Karl-Henry Victor[2], Newdeskarl Saint-Fleur[2], Lena Cauchie[1], Dominique Boisson[2], Claude Prépetit[5]

[1]University of Liege, Department of Geology, Georisk and Environment, Liege, 4000, Belgium

[2]Université d'Etat d'Haïti, Faculté des Sciences, LMI-CARIBACT, URGéo, Port-au-Prince, 10 Impasse Ambroise, Haiti

[3]Centre Spatial de Liège, Liege, 4000, Belgium

[4]University of Liege, Department of Urban & Environmental Engineering, Applied Geophysics, Liege, 4000, Belgium

[5]Unité Technique de Sismologie, Bureau des Mines et de l'Energie, Port-au-Prince, Delmas 31, Haiti

[6]TU Berlin, Faculty VI Planning Building, Environment Department of Engineering Geology, Berlin, 1587, Germany

Correspondence to: Hans-Balder Havenith (hb.havenith@uliege.be)

https://doi.org/10.5194/nhess-2022-83
Preprint. Discussion started: 9 March 2022

Natural Hazards and Earth System Sciences
Discussions

Abstract. First analyses of landslide distribution and triggering factors are presented for the region affected by the August, 14, 2021, Nippes, earthquake (Mw=7.2) in Haiti. Landslide mapping was mainly carried out by comparing pre- and post-event remote imagery (~0.5 -1-m resolution) available on Google Earth Pro® and Sentinel-2 (10-m resolution) satellite images. The first covered about 50% of the affected region (for post-event imagery and before completion of the map in January 2022), the latter were selected to cover the entire potentially affected zone. On the basis of the completed landslide inventory, comparisons are made with catalogues compiled by others both for the August 2021 and the January 2010 seismic events, including one open inventory (by the United States Geological Survey) that was also used for further statistical analyses. Additionally, we studied the pre-2021 earthquake slope stability conditions. These comparisons show that the total number of landslides mapped for the 2021 earthquake (7091) is smaller than the one observed by two other research teams for the 2010 event (e.g., 23,567, for the open inventory). However, these fewer landslides triggered in 2021 cover much wider areas of slopes (>80 km^2) than those induced by the 2010 event (~25 km^2 – considering the open inventory). A simple statistical analysis indicates that the lower number of 2021-landslides can be explained by the 'under-mapping' of smallest landslides triggered in 2021, partly due to the lower resolution imagery available for most of the areas affected by the recent earthquake; this is also confirmed by an inventory completeness analysis based on size-frequency statistics. The much larger total area of landslides triggered in 2021, compared to the 2010 earthquake, can be related to different physical reasons: a) the larger earthquake magnitude in 2021; b) the more central location of the fault segment that ruptured in 2021 with respect to coastal zones; c) and possible climatic preconditioning of slope stability in the 2021-affected area. These observations are supported by (1) a new pre-2021 earthquake landslide map, (2) rainfall distribution maps presented for different periods (including October 2016 - when Hurricane Matthew had crossed the western part of Haiti), covering both the 2010 and 2021 affected zones, as well as (3) shaking intensity prediction maps.

1 Introduction

This paper presents a first overview of landslide hazard induced by the August 14, 2021, Nippes (Haiti) earthquake. The epicenter (18.434° N / 73.482° W, hypocentral depth of 10 km) of this event is located

https://doi.org/10.5194/nhess-2022-83
Preprint. Discussion started: 9 March 2022

Natural Hazards and Earth System Sciences
Discussions

in the western part of the southern Haitian peninsula (see Unites States Geological Survey, USGS, Earthquake Hazard Program page, earthquake.usgs.gov, presenting first information on the 2021 M 7.2 - Nippes, Haiti, event). Similar to the January 12, 2010, earthquake, the epicenter is located near the surface expression of the Enriquillo-Plantain-Garden Fault (EPGF) that crosses the peninsula from East to West, marking one of the highest seismic hazard zones of the island (see location of the epicenters on the seismic hazard map completed by Frankel et al. in 2011, as well as on the topographic map shown in Fig. 1).

For the 2010 event, Calais et al. (2010) and Symithe et al. (2013) showed that this earthquake was caused by the oblique rupture of a formerly unknown fault dipping towards the North and located immediately in the North of the EPGF. Data provided by the earthquake.usgs.gov webpage (considering the provided moment tensor solution; see also Okuwaki and Fan, 2022) indicate that the situation could be similar for the 2021 event, with a ruptured fault segment dipping towards the North, and mostly located in the North of the EPGF. Thus, also the recently ruptured fault segment would not belong to the EPGF (which is essentially a left-lateral strike-slip fault). It could be related to an adjacent blind fault segment with oblique slip character (left-lateral strike-slip combined with reverse movement) according to the information available on earthquake.usgs.gov. As by now there is no clear answer to this question, below we will use the term of the 'EPGF zone' that includes the main strike-slip fault and annexed oblique slip fault segments (the two that are now known, i.e., the one ruptured in 2010 and the one that produced the last earthquake) to denominate the tectonic structure that produced those two events.

Even though the magnitude of the 2021 earthquake is slightly larger than the one of 2010 (Mw=7.2 and Mw=7.0, respectively, see information on the earthquake.usgs.gov webpage and by Stein et al., 2021), the recent event was far less catastrophic as it hit a less populated area compared to the 2010 earthquake that occurred just near the western entrance of the capital of Haiti, Port-au-Prince. The 2021 earthquake accounts for about 2250 fatalities (2/3 of which occurred in the provincial city of Les Cayes, located in Fig. 1), while the 2010 death toll is up to 300,000. However, it quickly became clear that the last event caused widespread slope failures that could be more intense than in 2010. Therefore, members of our research teams completed some ground control during field visits along segments of important roads hit by rock falls near the epicentral region. Additionally, we mapped all landslides visible on high-resolution (<=1 m) satellite imagery available on Google Earth Pro® (GEPro, zooming to a scale of about 1/2500),

https://doi.org/10.5194/nhess-2022-83
Preprint. Discussion started: 9 March 2022


Natural Hazards and Earth System Sciences
Discussions
Open Access
EGU

starting from August 28, 2021 (the first post-seismic high-resolution imagery available on GEPro), until the end of October 2021 (comparing also with available pre-2021 imagery). This study was complemented by landslide identification on Sentinel-2A and 2B products (10-m spatial resolution) sensed for the period from August 14, 2021, until the end of September 2021 (especially for areas not covered by higher resolution imagery on GEPro). This way, we could map landslides over the whole area potentially hit by the 2021 event by using this imagery, as it will be explained in section 2.

After completion of the 2021 landslide inventory, statistical characteristics of the latter were compared with equivalent results obtained for the 2010 USGS catalogue by Harp et al. (2016); some statistical data are also compared with those of one other inventory completed by Martinez et al. (2021, USGS Open File report) for the 2021 event and of two additional catalogues compiled for the 2010 event (by Gorum et al., 2013 and Xu et al., 2014). A size-frequency analysis was carried out to assess the inventory completeness (using the method proposed by Malamud et al., 2004) for our 2021 and the USGS open 2010 landslide catalogues.

We also mapped landslides existing before the 2021 earthquake by using high-resolution (<=1 m) imagery available on GEPro starting from October 2014 until the end of 2017, to study some preconditioning of slope instability that was induced in 2021. In particular, it is known that the region is regularly affected by hurricanes – the last catastrophic hurricane had impacted the target area in October 2016: 'Matthew' or 'Mathieu' in French (see track roughly outlined in Fig. 1b). Also, just two days after the main shock, on August 16, another Hurricane, 'Grace', hit the area and hampered help convoys to reach the areas most impacted by the earthquake. Right after this event, it was not immediately clear if 'Grace' had contributed to landslide activity or not; this question will be analyzed in the following sections by comparing landslide distributions with monthly precipitation maps produced by the 'Global Precipitation Measurement' (GPM) Mission (NASA) for different periods.

https://doi.org/10.5194/nhess-2022-83
Preprint. Discussion started: 9 March 2022

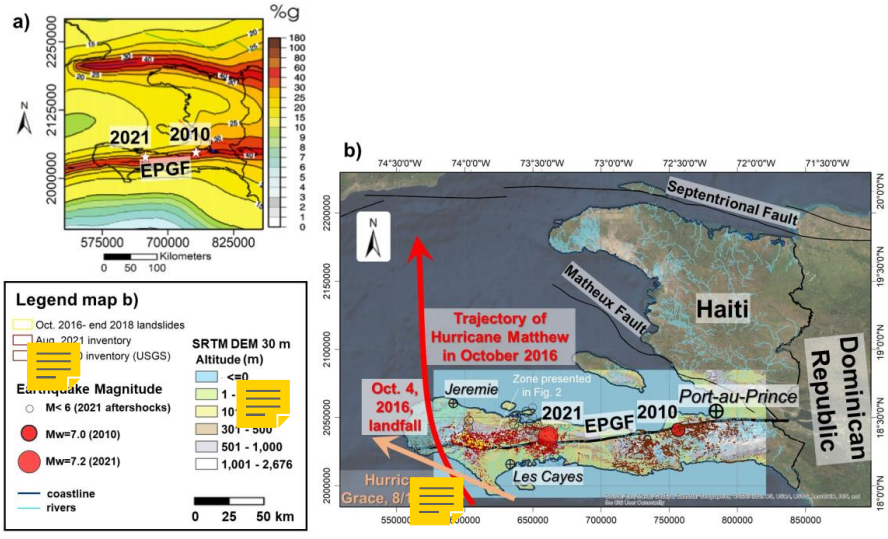

Figure 1: Location of the study region in Haiti. a) Seismic hazard map of Haiti (modified from Frankel et al., 2011) with location of the January 12, 2010, and August 14, 2021, main epicenters. b) Topographic map of Haiti (by © ESRI) 'with study region highlighted. See also location of the 2010 and 2021 epicenters and of the cities with the largest number of victims caused by each of the events (the capital Port-au-Prince, hit in 2010 and the provincial city of Les Cayes with largest effects in 2021), the outline of the main active fault system in the southern part of Haiti, the Enriquillo-Plantain-Garden-Fault (EPGF), and indication of the approximate trajectory of Hurricane Matthew in October 2016. Landslides mapped by Harp et al. (2016) are shown by brownish polygons (near the 2010 M=7 epicenter), and recently mapped landslides triggered in August 2021 are outlined in dark red (mainly in the West and South of the 2021 epicenter). Other digital outlines, including faults and coastline, were provided by the Centre National de l'Information Géo-Spatiale (CNIGS) of Haiti. See also location of the zone presented in Fig. 2.

Finally, we also present a comparison of the 2010 and 2021 landslide distributions with respect to Arias Intensity (Ia, see Arias, 1970) prediction maps, computed for each event by using the attenuation law proposed by Keefer and Wilson (1989).

https://doi.org/10.5194/nhess-2022-83
Preprint. Discussion started: 9 March 2022

Natural Hazards and Earth System Sciences
Discussions
Open Access
EGU

2 Methodological aspects of landslide and seismic trigger factor mapping

2.1 Landslide mapping

Right after the main shock that hit Haiti on August 14, 2021(precisely at 12:29:08 UTC, about 8:30 am local time), it became clear that many landslides were triggered by this earthquake. Within a few hours after the main shock, there were reports about rock falls cutting the main road RN7 connecting the large provincial cities of Les Cayes in the South and Jeremy in the North. Therefore, members of our local research teams checked the situation to support local administration with cleaning the roads. Photographs of rock falls in the central part of the target area are shown in Fig. 2 (those shown below all occurred in limestone rocks), together with the locations of the affected sites on a map.

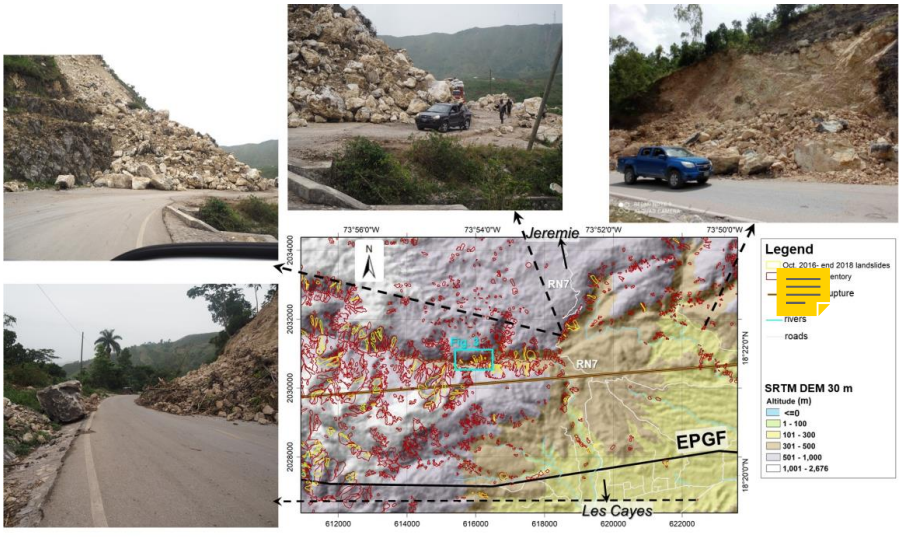

Figure 2: Examples of landslides photographed in the field, especially along the national road RN7, connecting the two provincial cities of Les Cayes in the South and Jeremy in the North. This map (located in the map of Fig. 1) also shows the different ground failure effects mapped before (yellow polygons) and after the earthquake (dark red polygons). See blue rectangle marking the outline of the view extent shown in Fig. 3, presenting a more detailed analysis of the co- versus pre-earthquake landslide activity. Other digital outlines, including rivers (light blue lines) and roads (white lines), were provided by the Centre National de l'Information Géo-Spatiale (CNIGS), Haiti.

https://doi.org/10.5194/nhess-2022-83
Preprint. Discussion started: 9 March 2022

These rock falls were typically not very large (with a volume of generally less than 20,000 m^3), but there were many of them and in some cases, it took several days before the street could be reopened. For that reason, our research groups, who have been working for several years on earthquake risk mitigation and communication in some areas hit by the 2021 event, started to detect and map all landslides caused by the earthquake. During field visits in August 2021, just after the main shock, our teams could confirm that this earthquake had triggered more extensive slope failures (covering wider surface areas) than the previous M=7.0 event in January 2010.

For the latter, several research groups had mapped co-seismic landslides (Gorum et al., 2013; Xu et al., 2014; Terrier et al., 2014, for urban areas and Harp et al., 2016). In the following section, a few statistical characteristics of the new 2021 landslide inventory are compared with those of the two first catalogues; a more detailed comparison is completed with the Harp et al. (2016) inventory, freely available online.

For the landslide mapping over the whole potentially affected area we have used medium-resolution imagery available from the Copernicus Open-Access Hub: Sentinel-2, with 10-m spatial resolution bands B2 (490 nm), B3 (560 nm), B4 (665 nm) and B8 (842 nm) collected for 8 different dates, every five to six days, between August 14, 2021 (the first one was available about two hours after the main shock), and the end of September 2021. Analyzing all images was necessary due to the extensive (but spatially variable) cloud cover present on each image. Considering that only this medium-resolution imagery was freely available in the beginning, we had decided to outline coalescent debris slides and flows marked by a main common part by one single coherent landslide polygon; this aspect will have to be taken into consideration when interpreting the landslide size-frequency statistics presented in the next section. As introduced above, during the following months, higher resolution (0.5-1 m) imagery became available on GEPro, which was then used to refine the initial landslide outlines, and to map smaller slope failures. At the end of October 2021 (and still in the beginning of 2022), about 50% of the potentially affected area was covered by higher resolution imagery (especially for the eastern part of this area). However, to maintain a coherence within the catalogue, the main rule to map coalescent slides with a major common part (and presenting the same aspect and type of failure) as one single mass movement was still respected. Examples of landslides mapped by applying this technique are presented in Fig. 3. Areas covered both by Sentinel-2 imagery and higher resolution images were also used to refine landslide mapping based on the first type of imagery, as by the end of 2021, only this one with 10-m resolution was available for the

https://doi.org/10.5194/nhess-2022-83
Preprint. Discussion started: 9 March 2022

Natural Hazards and Earth System Sciences
Discussions
Open Access
EGU

western zone (compare Fig. 3c and 3d). As a comparison with pre-event imagery was necessary in many cases to be sure that only 'co-seismic' (or nearly co-seismic – see explanation below) slope failures had been mapped, the whole area was screened by using high resolution (0.5-1 m) imagery available on GEPro for the period between 2014 and August 2021. A pre-earthquake image (of November 28, 2014) is shown in Fig. 3a, highlighting the contrast between the densely vegetated slopes present in the target region and the extensive denudation that occurred during the earthquake of August 2021 (see images shown in Figs. 3c and 3d). However, we could also observe by comparing multiple images available for the pre-event period that some denudation had already appeared for smaller zones before 2021. Zones marked by narrow debris slides and flows could be outlined especially on images available for the period between October 10, 2016 and the end of 2017. Fig. 3b presents an image of October 12, 2016 that shows the 'freshest' type of denudation since 2014 (see yellow polygons outlining such denudation zones), some of which disappeared after two years, due to revegetation of the slopes (rapid revegetation can be observed as the whole area is located in tropical regions). This image and others available for the same period were added to GEPro after Hurricane Matthew had impacted, in early October 2016, the same area as the one hit by the 2021 earthquake. The consequences of this 'double' impact on the target region will be analyzed in the sections 3 and 4 on the basis of precipitation distribution maps.

Actually, Haiti is quite often (at least once per year) crossed by hurricanes or tropical storms, some of which can trigger slope failures over wide areas. One such tropical storm that later developed into the hurricane called 'Grace' had also crossed southern Haiti, just two to three days after the August 14, 2021, main shock. We introduce this fact here in the methodological part as it had two consequences for the landslide mapping: first, right after the earthquake wide areas were covered by clouds during several days (some higher mountain parts even for weeks); thus, multiple satellite images of different dates (both Sentinel-2 and higher resolution imagery on GEPro had to be inspected to map landslides over the whole area. Second, we had to consider that 'Grace' might also have induced slope failures and that landslides mapped by using post-hurricane imagery were not all seismically triggered, or were at least enlarged by the effects of 'Grace'. Therefore, by comparing the post-seismic, August 14, Sentinel-2 image (collected before the Hurricane Grace event) with the one of August 29, 2021 (post-seismic and post-hurricane), we checked if additional or enlarged slope failures had appeared on the latter. An example of such a comparison is presented in Fig. 4, where red arrows point to zones marked either by new or by larger

https://doi.org/10.5194/nhess-2022-83
Preprint. Discussion started: 9 March 2022

Natural Hazards and Earth System Sciences
Discussions
Open Access
EGU

198 slope failures on the Sentinel-2 image of August 29, 2021, which were thus most likely caused by rainfall
199 during the Grace climatic event (disregarding here the possible additional influence of aftershocks
200 occurring during the same time in the region, which will be discussed below). Unfortunately, due to the
201 extensive cloud cover in mid-August 2021, such a comparison could only be completed for about 10%
202 of the seismically impacted area. For those cloud-free zones, we estimate that Grace had induced a
203 widening of slope denudation of about 10-15% compared to the purely seismically triggered slope
204 failures. As most images were available after the Grace event, the total number of 7091 landslides
205 mapped for the period between August 14 and the end of October 2021 inevitably also includes
206 precipitation-induced or reactivated slope failures (thus increasing the initial total number and area of
207 co-seismic landslides by about 10-15%). This aspect has also to be taken into consideration when the
208 landslide impact of the 2021 earthquake is compared with the one of 2010 (as analyzed in the next
209 section).

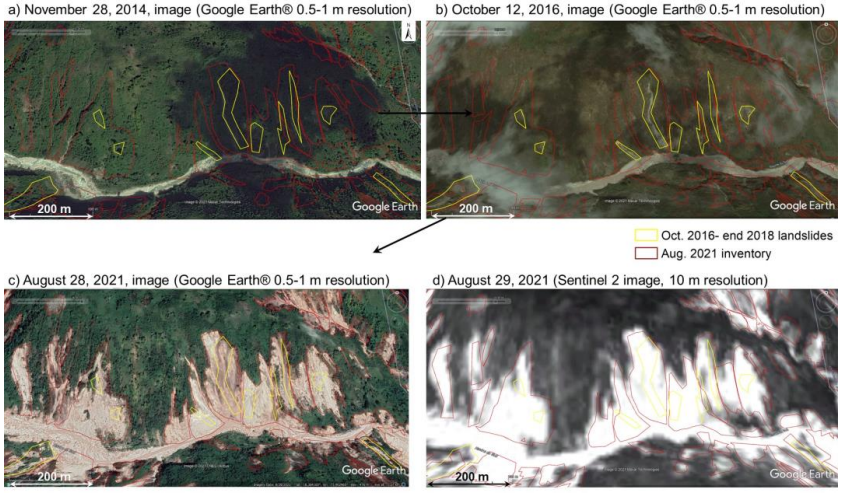

210

211 **Figure 3: Outlines of landslides mapped between October 2016 – November 2017 (in yellow; most by using**
212 **October 10-12, 2016, images, directly after Hurricane Matthew) and after August 14, 2021 earthquake (dark**
213 **red polygons), plotted on © Google Earth Pro, (a) high-resolution image available in GEPro for November 28,**
214 **2014, on (b) high-resolution image available in GEPro for October 12, 2016, on (c) high-resolution image**
215 **available in GEPro for August 28, 2021, and on (d) 10-m resolution Sentinel-2 image of August 29, 2021**
216 **(appearing in Black-White only in GEPro – in color in our GIS database).**

https://doi.org/10.5194/nhess-2022-83
Preprint. Discussion started: 9 March 2022

Natural Hazards and Earth System Sciences
Discussions

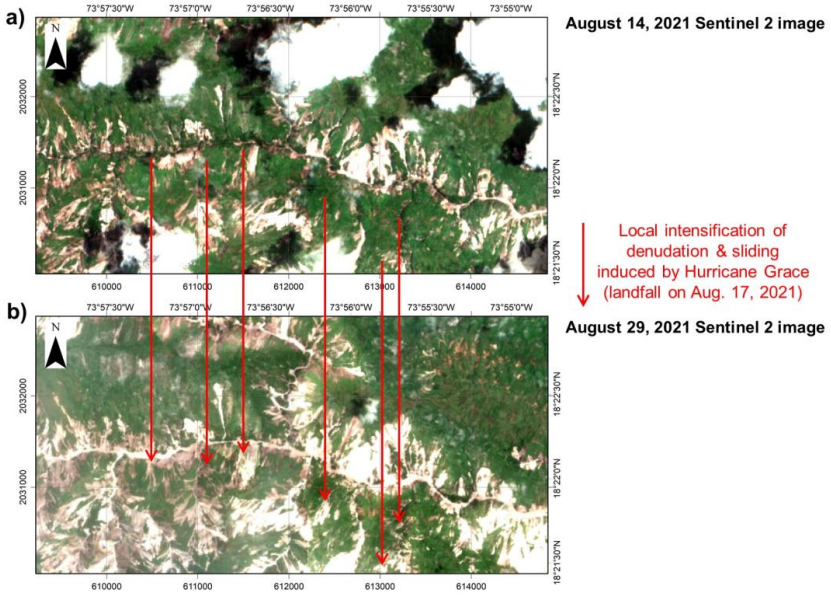

Figure 4: Comparison between Sentinel-2 images (10-m resolution) for the same area obtained for (a) August 14 (about 2h after the main shock) and for (b) August 28, 2021 (12 days after impact by Hurricane Grace that crossed the region on August 16, 2021). Red arrows point to zones where an intensification of denudation and sliding can be observed.

2.2 Landslide distribution statistics and size-frequency analysis

In sub-section 3.2, observed total landslide numbers and surface areas as well as other parameters characterizing the statistics of the two inventories, the new one presented here for 2021 and the one for 2010 by Harp et al. (2016), are compared with 'predicted' ones. The latter numbers are computed according to prediction laws proposed by Havenith et al. (2016) and Malamud et al. (2004). To estimate the total number (N_{LT}, see Eq. 1) of landslides triggered by a specific earthquake, Havenith et al. (2016) recommend to take into consideration the shaking intensity factor, (I, based on the Arias Intensity and thus on the earthquake magnitude, M; see Eq. 6b in the next sub-section), the fault factor F (depending on the type, FT, and size of the fault rupture, considering also the influence of a possible surface rupture), the topographic energy (TE, using mainly as parameter the maximum altitude difference in the affected

https://doi.org/10.5194/nhess-2022-83
Preprint. Discussion started: 9 March 2022

region), the climatic background (CB) conditions, and the lithological factor (LF, depending on the presence of soft soils for instance).

$$N_{LT} = 1000 \times I \times F \times TE \times CB \times LF \,, \quad (1)$$

Compared with the prediction of the total number of landslides triggered by a specific earthquake proposed by Havenith et al. (2016), the one recommended by Malamud et al. (2004) is much simpler (Eq. 2) and only based on the earthquake magnitude, M.

$$N_{LT} = 10^{(1.29M - 5.65)} \,, \quad (2)$$

For the calculation of the total area potentially affected by landslides (A_{Lext}, area within the maximum extent of landslide occurrence) Havenith et al. (2016) propose the following Eq. (3), which also directly considers the earthquake magnitude, M, and the hypocentral Depth, D:

$$A_{Lext} = I \times FT \times TE \times CB \times LF \times M \times D^2 \,, \quad (3)$$

As Havenith et al. (2016), Keefer and Wilson (1989) also propose an equation to estimate the total area potentially affected by landslides during one earthquake event. Their estimate of A_{Lext} is purely based on the earthquake magnitude, similar to Eq. (2) proposed by Malamud et al. (2004) to estimate N_{LT}:

$$A_{Lext} = 10^{(M - 3.46)} \,, \quad (4)$$

Malamud et al. (2004) do not propose any formula to estimate the total area potentially affected by landslides during an earthquake event as Havenith et al. (2016) (see Eq. 3), but recommend the following prediction law (Eq. 5) to estimate the total area effectively covered by co-seismic landslides, A_{LT}, based on the observed or predicted (using Eq. 2, or any other related prediction law, such as the one in Eq. 1) total number of landslides:

$$A_{LT} = 0.00307\, N_{LT} \,, \quad (5)$$

All the previous equations were used to compute the respective values presented in Table 1 in sub-section 3.2.

Size-frequency relations were computed for the 7091 landslide outlines in terms of frequency-density function (FDF) on the basis of the measured surface areas, $f(A_L)$. The same statistics were also computed for the 23,567 landslides mapped by Harp et al. (2016). Therefore, we used the method introduced by

https://doi.org/10.5194/nhess-2022-83
Preprint. Discussion started: 9 March 2022

Malamud et al. (2004) for surface areas (Eq. 6):

$$f(A_L) = \frac{\delta N_L}{\delta A_L} \quad (6)$$

where δN_L is the number of landslides with areas between A_L and $A_L + \delta A_L$ (representing the difference between two landslide surface area classes). Surface areas were calculated in km^2. Related distributions computed, respectively, for each landslide catalogue (for the 2010 one by Harp et al., 2016; and for the new 2021 inventory) are then compared with theoretical frequency-density distributions, as proposed by Malamud et al. (2004). The latter are based on the three-parameter inverse-gamma probability distribution (see equation 3 in Malamud et al., 2004) that is multiplied by the total number of landslides of simulated events (100, 1000, etc.). In this regard, it should be noted that the original technique proposed by Malamud et al. (2004) to complete the size-frequency statistics is based on the probability-density values, corresponding to the frequency-density values divided by the total number of mapped landslides, N_{LT} (which can be fit by the aforementioned three-parameter inverse-gamma probability distribution). However, as indicated above, due to the limited amount of high-resolution imagery available for the area potentially affected by seismic shaking in August 2021, not all small landslides could be mapped; therefore, the total number of landslides seismically triggered in August, N_{LT}, is likely to be higher than 7091 (even if the potential 'hurricane-effect' is removed, as explained below), and the probability-density function cannot be correctly computed. For such cases, Malamud et al. (2004) recommend the computation of the frequency-density function to assess the completeness of the inventory by comparison with the aforementioned predefined theoretical frequency-density functions, as it will be shown for the 2010 and 2021 inventories in the following section.

2.3 Mapping of seismic landslide triggering factors

Above, we highlighted the climatic influence on slope stability in the target area that must be taken into consideration when interpreting the landslide distribution statistics. However, it is obvious that for such an event the main trigger factors are still related to earthquake shaking; those have to be assessed to understand why extensive slope instability could be observed in one zone and only isolated minor failures occurred in another one. Such an analysis is completed both for the 2010 and 2021 events, by computing the Arias Intensity distribution maps (for 2010, comparing the results with the landslide distribution as

https://doi.org/10.5194/nhess-2022-83
Preprint. Discussion started: 9 March 2022


Natural Hazards and Earth System Sciences
Discussions

observed by Harp et al., 2016).

The Arias Intensity (Arias, 1970), Ia, can be considered as a quantitative measure of the degree of shaking (in m/s) on the surface. With respect to any other intensity characterization (including the one based on surveys) it has the advantage to be more objective and comparable for different earthquakes (according to Harp and Wilson, 1995). Wilson and Keefer (1985) were the first to try to correlate seismically triggered landslide distributions with this intensity measure. They also defined the following attenuation relationship (Eq. 7a) in terms of magnitude (M) and hypocentral distance (R):

$$\log(\mathrm{Ia}) = -4.1 + \mathrm{M} - 2\log(\mathrm{R}) + 0.5\mathrm{P} \quad , \tag{7a}$$

where P considers a possible deviation from the main law (P=0 stands for the average value).

Afterwards, Keefer and Wilson (1989) have reviewed the application of this formula and defined a new one (Eq. 7b), for magnitudes greater than 7:

$$\log(\mathrm{Ia}) = -2.35 + 0.75\mathrm{M} - 2\log(\mathrm{R}) \quad , \tag{7b}$$

We applied the latter equation as both the 2010 and 2021 can be considered as M>=7 events. The R-value represents the hypocentral distance map, here computed by using as source zone the blind fault rupture segments of the 2010 and 2021 events (with 0 km epicentral distance and 10 km hypocentral depth along the respective segment).

All equations introduced above have been applied to obtain the computation results presented below, in the sub-sections 3.2 and 3.4.

3 Results: landslide inventory statistics and analysis of trigger conditions

This section first summarizes a series of landslide type and general distribution characteristics. Second, landslide inventory and size-frequency statistics are presented and supported by an inventory completeness analysis. Third, a study of possible climatic slope failure preconditioning and post-seismic landslide surface changes is presented, which also compares landslide distributions with monthly precipitation maps (using output maps of the Global Precipitation Measurement Mission, GPM, produced by the NASA, for different periods, according to Acker and Leptough, 2007). Fourth, the landslide occurrence observed in 2010 and in 2021 is compared with respective shaking intensity prediction maps.

https://doi.org/10.5194/nhess-2022-83
Preprint. Discussion started: 9 March 2022

312 **3.1 Landslide type and distribution characteristics**

313 Before analyzing specific statistical values of the two landslide inventories, the one compiled by Harp et
314 al. (2016) for the 2010 event and ours completed after the August 2021 earthquake, we first have a look
315 at the general respective spatial landslide distributions and provide basic information on the type of the
316 mapped landslides.

317 The map presented in Fig. 5a shows that the global extent of landslides triggered in 2010 (brown outlines
318 within the brown maximum extent polygon) and in 2021 (dark red outlines within the dark red maximum
319 extent polygon) is quite similar (exact values are presented in Table 1). However, the 2010 landslide
320 distribution appears a bit more dispersed than the one of 2021 that is marked by two focal areas, one in
321 the southeastern part and one in the central western part of the total area affected in 2021. A major
322 difference between the two landslide distributions can be observed with respect to the location of the
323 EPGF zone. While most landslides occurred in the South of the fault zone in 2010, a relatively symmetric
324 distribution of landslides with respect to the location of the EPGF zone can be observed for the 2021
325 event. This is mainly due to the fact that the fault segment that ruptured near EPGF in 2010 is located
326 close to the coast (actually just in the South of the coast, as can be seen in the map in Fig. 5a), and thus
327 only limited onshore surface areas could be affected by landslides in the North of the EPGF zone in 2010,
328 while the location of the fault segment that ruptured in 2021 is more central within the southwestern
329 peninsula of Haiti.
330 Another important observation is that there seems to be a gap between the zone affected by landslides in
331 2010 and the one affected in 2021. This means that, according to our present observations, the 2021
332 earthquake did not reactivate landslides triggered in 2010 – due to the large distance (> 60 km) between
333 the fault ruptures. Actually, this point still has to be confirmed as the westernmost part of the area affected
334 by the 2010 earthquake shaking is not covered (since August 14, 2021, until January 2022) by higher
335 resolution imagery in GEPro. This check could only be done so far with the 10-m resolution Sentinel-2
336 imagery.
337

https://doi.org/10.5194/nhess-2022-83
Preprint. Discussion started: 9 March 2022

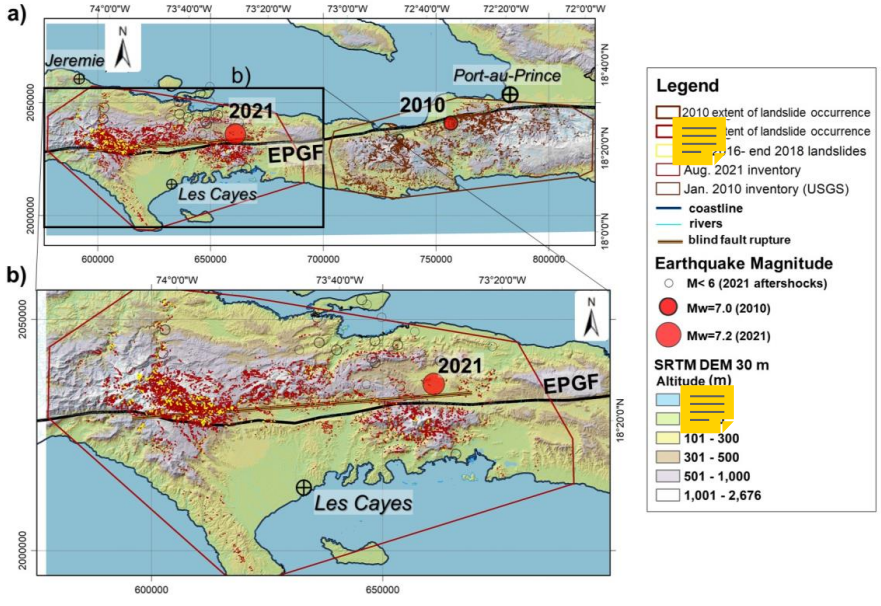

Figure 5: a) Study region with areas affected, respectively, by the two Mw >= 7 events. Individual landslides triggered in 2010 (Harp et al., 2016, inventory) are mapped as small brown polygons (appearing as points at this scale) and the maximum extent of landslides triggered in 2010 is outlined by the large brown polygon. Landslides mapped for the 2021 event are shown as small dark red polygons within the maximum landslide extent area outlined by the large dark red polygon. b) Focus on the region hit by the August 2021 earthquake, with 7091 landslide locations shown by dark red polygons. See also main shock and after-shock (empty circles) location (from earthquake.usgs.gov) and outline of the (roughly 80 km long) blind fault rupture (extracted from USGS page: https://earthquake.usgs.gov/earthquakes/eventpage/us6000f65h/finite-fault).

An important consequence of the specific location of the ruptured fault segments is that quite large landslides had occurred along the shore in 2010, where some of them had massively impacted the ocean and, thus, had produced up to 3 m-high Tsunami waves (see Olson et al., 2011; Poupardin et al., 2020; Fritz et al., 2013; Sassa and Takagawa, 2018) while there is not a single report of a major coastal landslide for the 2021 event – as the fault rupture occurred at a distance of minimum 10 km away from the nearest shoreline. Instead, a wider onshore area was exposed to high intensity earthquake shaking during the 2021 event. The related impact will be analyzed below on the basis of the statistical values presented in

https://doi.org/10.5194/nhess-2022-83
Preprint. Discussion started: 9 March 2022

Natural Hazards and Earth System Sciences
Discussions
Open Access
EGU

355 Table 1.

356 Concerning the types of landslides triggered by the 2021 earthquake, we can say that by far most of them
357 can be classified as debris slides or flows (see examples in the GEPro view presented in Fig. 6b) and as
358 medium-size (most with a volume of less than 20,000 m^3) rockfalls (as shown above in Fig. 2). Thus, at
359 least 95% of all landslides mapped are relatively shallow (with a depth of less than 15 m). Actually, not
360 a single large massive landslide (> $2*10^7$ m^3) could be identified. A similar observation was made by
361 Harp et al. (2016) for the landslides triggered in 2010 (see view in Fig. 6c). However, when comparing
362 individual landslides induced in 2021 with those triggered in 2010, the latter are almost systematically
363 narrower than those of 2021 (compare the very narrow slides and flows in Fig. 6c with the typically
364 wider ones in Fig. 6b), while located in similar geological (limestone) and topographic (hilly-
365 mountainous) environments. Actually, in the so-called Ravine du Sud (Gorge of the South), part of which
366 is shown above in Figs. 3 and 4, numerous very extensive slope failures (but still relatively shallow)
367 could be observed; most of them formed by coalescent neighboring debris slides. Thus, entire slope units
368 (delimited by upper and lateral slope crests and the valley bottom) finally collapsed as one single mass
369 movement. Such kind of extensive slope failures occurred far less frequently in 2010 – at least onshore,
370 while at least a few aforementioned coastal and mostly submarine landslides must have been quite
371 massive as their impact had triggered Tsunami waves, as indicated above.
372 The fact that no really massive landslides had occurred (onshore), both in 2010 and 2021, also explains
373 why only a few longer lasting landslide dams had formed on the rivers. We could identify only about 100
374 minor dams (with a volume of less than 50,000 m^3, according to our estimate) after the August 2021
375 main shock, most of which had disappeared before the end of October 2021; and, only a few dozens of
376 them were impounding temporary lakes. In this regard it should be noted that Martinez et al. (2021), who
377 had also mapped landslides triggered by the 2021 Nippes earthquake (4893, according to their open file
378 report), have outlined almost 300 (at least partial) landslide dams after the event. However, they also
379 indicate that most of them failed a few days after formation; still, at the time of publication of their open
380 file report in December 2021, they consider 35 of the remaining dams as potentially hazardous. Here, we
381 will not further analyze this aspect as any related hazard assessment would require a site-specific
382 approach that is not targeted by this first study completed at regional scale.

https://doi.org/10.5194/nhess-2022-83
Preprint. Discussion started: 9 March 2022

Natural Hazards and Earth System Sciences
Discussions
Open Access
EGU

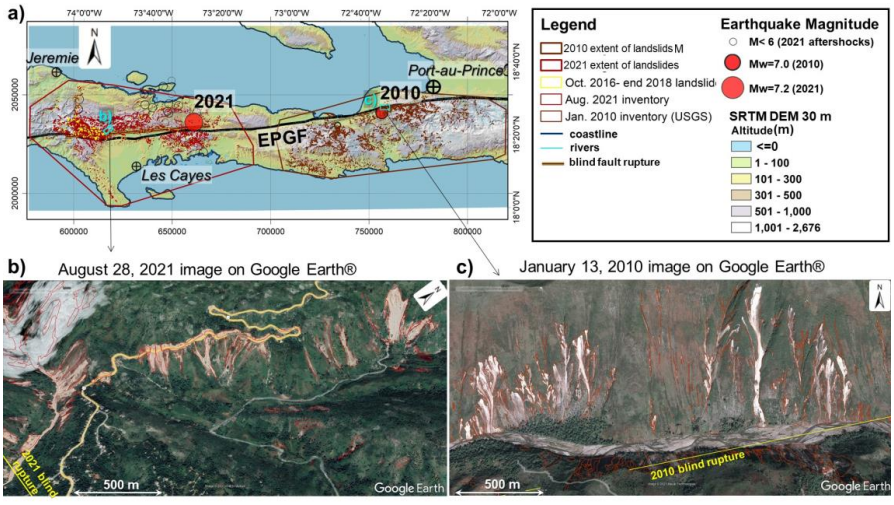

Figure 6: a) Landslide distribution map for the two events in 2010 and 2021. b) GEPro view (© Google Earth Pro) of landslides triggered by the August 2021 earthquake. c) GEPro view (© Google Earth Pro) of landslides induced by the January 2010 main shock (with landslide outlines by Harp et al., 2016).

While debris slides are the predominant type of 2021 slope failures in the central mountain ranges, widespread s[illegible]l slides (but of smaller volume, typically of less than 10,000 m^3) had occurred along the hills (with a crest alt[illegible]f less than 400 m) of the peninsula located in the Southwest of Les Cayes (southern part of map in Fig. 5b). As the slopes are very gentle, often seem to be less than 5°, it could be that those failures, many of which affected agricultural areas (marked by brownish disrupted fields), are related to liquefaction phenomena. However, also this observation has to be reexamined, by ground-control and site-specific studies, as the remote analysis based on 1-m resolution imagery does not allow us to fully confirm this interpretation.

3.2 Landslide inventory and size-frequency statistics

Table 1 presents an overview of landslide inventory statistics, for both the 2010 and 2021 events. The numbers in the first row show that apparently fewer landslides have been triggered in August 2021 (considering also the number of 4893 landslides published in the open file report by Martinez et al., 2021)

https://doi.org/10.5194/nhess-2022-83
Preprint. Discussion started: 9 March 2022

Natural Hazards and Earth System Sciences
Discussions

than in January 2010. At least two inventories, the one by Harp et al. (2016) and the one of Xu et al. (2014), include far more landslide outlines (23,567 for the first, 30,828 for the second) than our catalogue for 2021 (7091). Only the inventory by Gorum et al. (2013) that was the first one to be completed for the 2010 event contains fewer data (4490 points – not polygons - marking the landslide location). However, paradoxically, a much wider surface area is covered by the apparently fewer 2021 landslides (a total area of 84 km^2, see row 3 in Table 1) than by the more numerous 2010 landslides (sum of surface areas of about 25 km^2, calculated for the Harp et al., 2016, inventory). This discrepancy can first be explained by the fact that 2021 landslides could only be mapped from higher resolution imagery for about half of the potentially affected area (in the eastern part). For the western zone, only Sentinel-2 images were available until the end of 2021. Those 10-m resolution images typically do not allow for the (complete) mapping of landslides smaller than 1000 – 2000 m^2. The second reason is documented by the GEPro views in Figs. 3, 4 and 6, showing that in 2021 many primarily individual landslides merged to form one single wider mass movement – thus reducing the final number of single landslides; to this the aforementioned 'enlargement' effect of Hurricane Grace should be added, which might have contributed to the coalescence of numerous 'small' landslides to form fewer larger landslides. Such a coalescence of landslides seems to have occurred less frequently in 2010 (see parallel very narrow debris slides and flows in Fig. 6c). In addition, for the coalescent debris slides, the type of mapping applied by Harp et al. (2016) and most likely also by Xu et al. (2014) was different: they have created outlines for each single component of a debris slide, even if those components form together a larger mass movement. To better highlight the impact of the mapping technique and the availability of high-resolution imagery on the landslide inventory completeness, a size-frequency analysis is presented in the second part of this sub-section. Before, we first compare the observed landslide numbers with those predicted by Havenith et al. (2016) and Malamud et al. (2014), respectively, for the two earthquakes. As introduced above (see Eq. 1), according to Havenith et al. (2016), this number depends on the seismic intensity (I, using as input the Ia value computed for the respective earthquake magnitude), the fault factor (type, size and possible surface rupture), the topographic energy (maximum difference of altitudes in the affected area), the climatic background (in this case marked by tropical wet climate), and the lithological factor (here using an average type, for rocks in general). For the precise classification of the different factors, the reader is referred to Table 1 in Havenith et al. (2016). Here, we used the values presented below in Table 2

https://doi.org/10.5194/nhess-2022-83
Preprint. Discussion started: 9 March 2022

(considering both events in 2010 and 2021), which indicate the following:

1) the shaking intensity values, I=0.74, in 2010, and I=1 in 2021 are characteristic for the respective magnitudes (note, this factor can reach a value of up to 3.5 in the case of high-magnitude earthquakes, with Mw > 8);

2) the fault factor, F=2.25, can be considered as similar in both cases, marked by an oblique slip that occurred along a fault segment with a length of 50-100 km, with no clear surface rupture (note, F can reach a value of up to 6 in the case of a surface rupture of an activated reverse fault segment with a length of more than 300 km, such as observed for the Wenchuan earthquake in 2008);

3) the topographic energy value, TE=2, in both cases characterizes a surface morphology marked by local altitude changes of more than 500 m within a hilly region (only smaller mountains, with an altitude of less than 2500 m can be found in the regions affected by the 2010 and 2021 events; note, Havenith et al., 2016, selected a value 4 to mark the high steep slopes in the Longmenshan Mountains affected by the Wenchuan earthquake in 2008);

4) the climatic background factor, CB=1.5 marks relatively wet conditions for the 2021 event while CB=1 indicates average conditions for the 2010 event (the higher value chosen for 2021 considers some preconditioning of slope instability by Hurricane Matthew, as explained in the next section; note, Havenith et al., 2016, selected a value CB=2 for the very wet conditions that can be found in the Longmenshan Mountains affected by the Wenchuan earthquake, characterized by yearly precipitation values of more than 3000 mm – while the target areas in Haiti are marked by values of about 2000 mm);

5) the lithological factor, LF=2, indicates that both weathered rocks and soft soils can be found in the affected area (note, Havenith et al., 2016, selected a maximum value, LF=4, for the Haiyuan-Gansu-Ningxia earthquake event, China, in 1920, as it affected an area that is almost entirely covered by Loess deposits, which are highly susceptible to slope failure).

When these different factor values are combined according to Eq. (1) presented above, the total numbers of landslides, N_{LT}, predicted for the 2010 and 2021 events are, respectively, 6694 and 13,476. These values can be compared with the numbers predicted by the simple equation (Eq. 2), proposed by Malamud et al. (2004), using only the earthquake magnitude as input: 2399 for the 2010 event and 4345 for the 2021 event. The latter prediction seems to clearly underestimate the observed numbers of triggered landslides, while those predicted by using Eq. (1) by Havenith et al. (2016) provide intermediate

https://doi.org/10.5194/nhess-2022-83
Preprint. Discussion started: 9 March 2022


Natural Hazards and Earth System Sciences
Discussions

458 values: larger than the number observed by Gorum et al. (2013) but smaller than the numbers observed
459 by Harp et al. (2016) and by Xu et al. (2014). The two predictions (Eq. 1 and 2) were also applied to the
460 2021 event; the first one producing a higher N_{LT} (=13,476) than the observed value, the second one
461 producing a lower value (=4345).
462 As shown on the maps in Fig. 5, also the total area within the maximum extent of landslide occurrence,
463 A_{Lext}, was outlined and then measured for the 2010 and 2021 events. The latter is about 1.4 times larger
464 than the first: 5100 km^2 for 2021 against 3700 km^2 for 2010. These values can be compared in Table 1
465 with the predictions by Havenith et al. (2016) and by Keefer and Wilson (1989), corresponding,
466 respectively, to 3124 and 3467 km^2, for the 2010 event, and to 6470 and 5495 km^2, for the 2021 event.
467 In this case, the very simple equation proposed Keefer and Wilson (1989) provides an estimate of A_{Lext}
468 that is closer to the observed value than the one produced by the more complex relationship proposed by
469 Havenith et al. (2016).
470 The third row of Table 1 compares the total observed slope areas affected by landslides, A_{LT},
471 corresponding, respectively, to a value of 24.86 km^2 for the 2010 event and of 84.38 km^2 for the 2021
472 event, with the values predicted by Eq. (5) by Malamud et al. (2004) for each event. For 2010, we applied
473 this relationship to the three observed values indicated in the first row and by using the N_{LT}, predicted
474 respectively by Havenith et al. (2016) and Malamud et al. (2004). Among all total landslide surface area
475 values predicted for the 2010 event, it can be seen that the one based on the Havenith et al. (2016) N_{LT}
476 estimate produces the best fit (=20.55 km^2) when compared with the observed value of 24.86 km^2. For
477 2021, the respective predictions all underestimate the observed total landslide surface area value, A_{LT}, by
478 a factor of at least two, even when the highest N_{LT} estimate (using Eq. 1) by Havenith et al. (2016) is
479 used.
480 The fourth and fifth rows show the average and median landslide surface area values, respectively, for
481 the 2010 landslide inventory by Harp et al. (2016) and the new 2021 inventory. Those values are clearly
482 higher for the last inventory, confirming on the one hand that larger landslides were triggered in 2021,
483 and, on the other hand, that many more small landslides were mapped by Harp et al. (2016) than by our
484 team for 2021. Especially the large difference between the median landslide surface area values (the 2021
485 value is almost twenty times larger than the 2010 value) highlights the 'mapping-related' factor, which
486 becomes obvious when considering the values in the next four rows. On the one hand, the smallest

https://doi.org/10.5194/nhess-2022-83
Preprint. Discussion started: 9 March 2022


Natural Hazards and Earth System Sciences
Discussions

487 landslide mapped by Harp et al. (2016) has a surface area of 0.5 m^2 and their inventory contains 6587
488 landslide polygons smaller than 100 m^2 while our inventory for 2021 only includes one landslide with a
489 surface area smaller than this value. On the other hand, the largest landslide mapped for the 2021 event
490 (>400,000 m^2) has almost twice the size of the largest one that occurred in 2010, when actually only 2
491 landslides larger than 100,000 m^2 had been triggered; in 2021, we could outline more than 100 landslides
492 larger than this value.
493 Finally, Table 1 provides information about the distribution of the 2010 and 2021 landslides with respect
494 to the blind fault rupture projected on the surface (near the EPGF outline). As already introduced above,
495 a much larger number of landslides occurred in the North of the latter in 2021 (=4678) compared to 2010
496 (=2548, at least for onshore slope failures); consequently, more landslides occurred in 2010 in the South
497 of the respective blind fault rupture. As the total number of mapped landslides is much larger for the
498 2010 event, the difference between those numbers is very high: 21,019 occurred in the South of the fault
499 rupture in 2010 and only 2420 in the South of the respective fault rupture in 2021. However, when the
500 total surface area affected by landslides is considered, the 2021 event affected more zones both in the
501 South and the North of the fault rupture than the 2010 event, while the distribution of landslides for each
502 event with respect to the fault rupture remains the same also when considering the affected surface areas:
503 they are much larger in the South of the fault rupture for the 2010 event but larger in the North for the
504 2021 event. The main explanation for this difference has already been provided above: the fault segment
505 that ruptured in 2010 is located close to the coast, with limited onshore surface areas being exposed to
506 landslide activity in the North of the respective fault rupture, while the location of the fault rupture in
507 2021 is more central with respect to the shorelines of the southwestern peninsula of Haiti. Actually, the
508 presence of more numerous and larger landslides in the North of the fault rupture of 2021 could be
509 expected, according to the observations made by Fan et al. (2018) for the Wenchuan earthquake in 2008,
510 which had triggered far more landslides on the hanging wall of the activated reverse fault segments than
511 on the foot wall. Considering the oblique slip character along the fault ruptures of 2010 and 2021 dipping
512 to the North, the hanging wall is located on the northside of the blind fault rupture projected on the
513 surface and would logically host more landslides (as indeed observed for the 2021 event). Thus, if a
514 larger 'onshore hanging wall' surface area (marked by a hilly or mountainous morphology) had been
515 available onshore for the 2010 event, it can be assumed that even more landslides would have been

https://doi.org/10.5194/nhess-2022-83
Preprint. Discussion started: 9 March 2022

Natural Hazards and Earth System Sciences Discussions

516 triggered (onshore). Now, we can only assume that in addition to the few known coastal failures also
517 massive submarine landslides must have occurred in the North of the 2010 fault rupture.

518

519 **Table 1: 2010 and 2021 landslide inventory characteristics – where not specified for the 2010 event, using the**
520 **Harp et al. (2016) inventory. The largest values for each specific observation/estimate (if more than 1 indicated)**
521 **are bold.**

Landslide inventory parameters/predictions	2010, Mw=7.0	2021, Mw=7.2
Observed number of landslides, N_{LT}	>4490[a] / 23,567[b] / **30,828**[c]	**7091**/4893[d]
Havenith et al. (2016) N_{LT} prediction 1	6694	13,476
Malamud et al. (2004) N_{LT} prediction 2	2399	4345
Area of region potentially affected by landslides, A_{Lext} (km^2)	3700	5100
Havenith et al. (2016) A_{Lext} prediction 1	3124	6470
Keefer and Wilson (1989) A_{Lext} prediction 2	3467	5495
Total surface area of landslides, A_{LT2} (km^2)	24.86	84.38
Malamud et al. (2004) A_{LT} prediction :		
for the observed N_{LT}	13.8[a] / 72.3[b] / **94.6**[c]	21.8
for the N_{LT} prediction 1	20.55	41.4
for the N_{LT} prediction 2	7.36	13.3
Average area (m^2)	1055	11,886
Median area (m^2)	254	4729
Smallest landslide (m^2)	0.5	75
Number of landslides smaller than 100 m^2	6587	1
Largest landslide (m^2)	234,370	409,479
Number of landslides larger than 100,000 m^2	2	103
Total number of landslides in the North (N) / South (S) of the fault rupture	N= 2548 **S= 21,019**	**N= 4678** S= 2420
Total surface area of landslides in the N / S of the fault rupture (km^2)	N= 2.45 **S= 22.41**	**N= 58.31** S= 26.07

522 [a] Number of landslides observed by Gorum et al. (2013), [b] by Harp et al. (2016), [c] by Xu et al. (2014),
523 and [d] by Martinez et al. (2021).

524

525 In addition to the numbers shown in Table 1 and explained above, we also provide two values for the

https://doi.org/10.5194/nhess-2022-83
Preprint. Discussion started: 9 March 2022

smaller landslide inventory compiled for the period between October 10, 2016 and the end of 2017. For this period, 324 landslide zones have been outlined (see yellow polygons shown on the views and maps in Figs. 3 and 5), covering a total surface area of 7.92 km^2. However, we must indicate that these values represent approximations as the main focus was on the identification and the determination of the general extent of those pre-2021 slope failures rather than on their detailed mapping.

Table 2: Factors contributing to the total number and surface area of landslides triggered by the 2010 and the 2021 earthquakes, according to the prediction proposed by Havenith et al. (2016). The minimum and maximum values proposed by Havenith et al. (2016) are also indicated, the latter with information on the event – region, to which this maximum factor value was attributed.

Haiti Events/ Factors	Shaking Intensity, I	Fault Factor, F (type, FT)	Topographic Energy, TE	Climatic Background, CB	Lithological Factor, LF	Hypocentral Depth, D (km)
2010	0.74	2.25(1.5)	2	1.5	2	10
2021	1	2.25(1.5)	2	1	2	10
min. values	0.1	0.75	1	0.5	1	10
max. values (event - region)	3.4 (Chile, 1960)	6 (Wenchuan, 2008)	4 (Wenchuan, 2008)	2 (Wenchuan, 2008)	4 (Haiyuan-Gansu-Ningxia, 1920)	226 (Hindu Kush, 2002)

Considering the values presented in Table 1, we still have to explain why the total surface area covered by landslides in 2021 is much larger than the one covered by the 2010 landslides: a) the first obvious physical reason for the larger area hit by mass movements in 2021 is the higher triggering earthquake magnitude of the last event (this effect will also be analyzed below by comparing the influence of shaking intensity on landslide susceptibility); b) another physical reason could be the possibly higher susceptibility to mass movements of the western part of the peninsula hit by the 2021 event, compared to the eastern part (this factor still has to be analyzed on the basis of landslide susceptibility maps, considering also the geological influence, which have been computed and will be presented in another paper); c) a third reason for the larger area affected by landslides in 2021 could be related to the aforementioned 'hurricane' effects that will be analyzed in the following sub-section; d) and fourth, the more central location of the fault segment activated in 2021 with respect to the coasts of the peninsula could also explain the larger (subaerial) slope failures triggered during the last event within the wider

https://doi.org/10.5194/nhess-2022-83
Preprint. Discussion started: 9 March 2022

Natural Hazards and Earth System Sciences
Discussions

onshore hanging wall part, as already introduced above.

However, we also have to admit that a small percentage of the larger landslide surface area mapped for the 2021 event could be related to the aforementioned technique of outlining coalescent landslides as single ones, where small unaffected areas have been included within the landslide polygon. For instance, this 'over-mapping' of landslide areas became obvious after the first rapid mapping session, only based on Sentinel-2 imagery. Thus, during the later refinement and splitting of the landslide polygons (using the higher resolution imagery that became available on GEPro), wide surface areas initially mapped within the landslide polygons were then excluded from them. Interestingly, the total surface area could not be reduced by this refinement (the initial total surface area covered by landslide polygons was about 75 km^2, which increased to 84 km^2, as shown in Table 1), as during the second mapping phase also numerous new smaller landslides could be mapped, the total area of which more than compensated the reduced area of the refined initial landslide polygons.

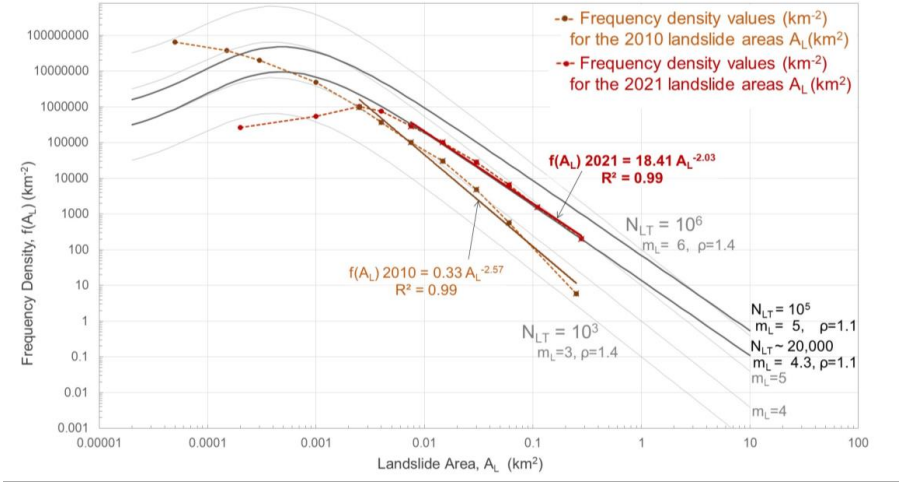

Figure 7: Frequency density graphs developed for the 2010 (in brown, by Harp et al., 2016) and the new 2021 landslide inventories (in dark red), compared with landslide frequency-density curves computed for different landslide event magnitudes according to equation 3 in Malamud et al. (2004). For computing the light gray curves, the decay exponent determined by Malamud et al. (2004) was used (=-2.4, = -(ρ+1)), while for the dark gray curves an exponent of -2.1 was used (similar to the one obtained for the 2021 landslide frequency-density distribution).

https://doi.org/10.5194/nhess-2022-83
Preprint. Discussion started: 9 March 2022

Natural Hazards and Earth System Sciences
Discussions
Open Access
EGU

567

568 To better quantify the 'mapping effect' on the landslide distribution statistics, we carried out an inventory
569 completeness analysis as proposed by Malamud et al. (2004), by computing and plotting frequency-
570 density values for various landslide surface area classes as shown on the graph in Fig. 7. Related curves
571 are compared with theoretical frequency-density distributions computed for various simulated landslide
572 events, composed, respectively of 1000, 10,000, 100,000 and 1,000,000 elements, here marked by the
573 landslide event magnitudes, m_L (3 to 6), corresponding to the logarithm (with base 10) of these values.
574 There are two important parameters to be analyzed for the observed frequency-density distributions,
575 through comparison with the theoretical curves: the first part is represented by the power-law decay (see
576 introduction in Stark and Hovius, 2001) that appears as a linear decay in the log-log graph below; the
577 second part is the so-called 'rollover', which can be observed for a landside surface area where the
578 exponentially decreasing number of larger landslides turns into a decrease of the number of smaller
579 landslides. According to Malamud et al. (2004) the main parameters characterizing these two parts should
580 be identical for all landslide events: the decay of larger landslide numbers should have an exponent-value
581 of about -2.4 (=-(ρ+1) for ρ=1.4, being the parameter controlling the power-law decay), which was used
582 for the calculation of the light gray theoretical frequency-density curves, while the rollover should occur
583 for all landslide events within the same landslide size class, marked by a surface area of about 400 m^2.
584 While a power-law decay can indeed be observed for both landslide inventories, the exponents
585 characterizing this decay slightly differ from the value of -2.4 that Malamud et al. (2004) had determined
586 for other inventories: for the 2010 inventory, the related absolute value is slightly higher (-2.57, for the
587 brown line fitting the 2010 data) and for the 2021 inventory it is clearly lower (-2.03, for the red line
588 fitting the 2021 data). Concerning the rollover, the 2010 landslide frequency-density distribution
589 interestingly does not present any such feature, while the 2021 inventory is marked by a rollover that
590 occurs for a landslide size class of about 3000 m^2. The comparison of this value with the much smaller
591 value determined by Malamud et al. (2004) clearly hints at the incompleteness of the 2021 inventory, at
592 least for the smaller landslides. To estimate this incompleteness, the part of the power-law decay
593 (supposed representing the 'complete' part of the landslide inventory) has to be compared with the
594 theoretical frequency-density curves of the simulated landslide events with various magnitudes (light
595 grey lines in the graph in Fig. 7). According to this comparison, the 2021 landslide event would have a

https://doi.org/10.5194/nhess-2022-83
Preprint. Discussion started: 9 March 2022

magnitude, m_L, close to 5 (=100,000 landslides!). For the 2010 event, the same comparison indicates a magnitude, m_L, close to 4 (=10,000 landslides!). While the theoretical landslide event magnitude of the 2021 event seems to largely overestimate the observed number of landslides, the one obtained for the 2010 event seems to underestimate the observed total number of landslides. Actually, the multiple predictions presented in Table 1 for the 2010 event also underestimate the high numbers of landslides observed by the two teams of Harp et al. (2016) and of Xu et al. (2014). Combining this comparison with the fact that the landslide inventory of Harp et al. (2016) does not present any rollover, and includes even more than 6000 landslides with a surface area smaller than 100 m^2, this catalogue (and possibly also the one of Xu et al., 2014) can be considered as 'superfine' – at least, when compared with the type of landslide distributions (and related mapping of individual slope failures) analyzed by Malamud et al. (2004). And this 'subtle refining' of the landslide outlines, partly related to the separate mapping of landslide zones that are coalescent, may also explain the higher exponent value of the power-law decay of the 2010 landslide frequency-density distribution as well as the high number of mapped landslides compared to all predicted values (see Table 1). In contrast, the rollover observed for a much larger landslide size class than the one predicted by Malamud et al. (2004), the smaller decay exponent (-2.0 instead of -2.4) obtained for our 2021, and the smaller observed total landslide number values compared to the one predicted by Havenith et al. (2016), all confirm the incompleteness of the latter catalogue, at least for landslides smaller than 3000 m^2. In the discussion part, some tools to remediate this problem in the future will be presented. However, as proposed by Malamud et al. (2004), by comparing the frequency-density distribution with the theoretical curves, an estimate of the actual total number of landslides could be made. As introduced above, the one of the 2021 event would be close to 100,000. Here, we will first propose a comparison with the same type of theoretical frequency-density curves, but computed for a decay exponent of -2.1, similar to the one of decay of the observed 2021 landslide frequency-density distribution. The graph in Fig. 7 shows that the 2021 data are best fit by such a curve representing an inventory of 20,000 landslides. Actually, a similar value could also be obtained for an exponent of -2.4 if we consider a lower number of large landslides that would in fact be composed of smaller ones (the weight of the latter would then increase and the one of the larger ones decrease, which leads to a stronger decay). Below we will discuss, which assumption would be the best: (1) that really 100,000 landslides might have occurred in 2021, or (2) that the decay exponent value of -2.4 is indeed

https://doi.org/10.5194/nhess-2022-83
Preprint. Discussion started: 9 March 2022


Natural Hazards and Earth System Sciences
Discussions

not as 'universal' as proposed by Malamud et al. (2004), or (3) that a future refinement of the 2021 landslide inventory would result in a frequency-density distribution marked by a higher (absolute value of the) decay exponent, close to -2.4.

3.3 Climatic (pre- and post-seismic) conditioning of slope instability

The climatic influence on landslide occurrence (in 2021) has been introduced above, by considering the possible impacts of hurricanes on slope failure occurrence, marked both by preconditioning of slope instability and by post-seismic intensification. We first start analyzing the last effect, by considering the potential impact of Hurricane Grace on post-seismic landslide intensification, on August 16-17, 2021 (when it had crossed the target region and was actually classified as tropical depression at that stage). A possible effect of related rainfalls on landslide occurrence has already been highlighted, for instance, on the AGU Landslide blog (by Petley, D., 2021, on blogs.agu.org/landslideblog). This effect could be confirmed when we compared Sentinel-2 imagery collected right after the earthquake (2h after the main shock) with images remotely sensed after August 17, 2021. As indicated above and shown in Fig. 4, an intensification of denudation could indeed be observed after the tropical storm Grace event. However, one important limitation has to be highlighted: this comparison could only be completed for about 10% of the area potentially hit both by the earthquake and by Grace, due to the intense cloud cover present in the target region during that period. Furthermore, another effect could have contributed to slope failure intensification after the main shock on August 14, the one related to the aftershocks (see empty circles shown in all maps above), but analyzing this effect would require a refinement of the satellite image analysis both in space and time, which is hardly possible considering the extensive cloud cover present in the target area when all those seismic shocks occurred. Here, we will focus on the possible climatic influence, which can better be outlined when comparing the landslide distribution with actual precipitation maps. Therefore, we used the Global Precipitation Measurement Mission (GPM, by NASA) data obtained via the https://giovanni.gsfc.nasa.gov/ website, corresponding to the merged satellite-gauge monthly precipitation estimate (in mm), assessed with a resolution of 0.1°. Related maps were requested for all months between August 2000 and July 2021, and also for the specific months of October 2016 and August 2021, as well as for all October months between 2000 and 2020. However, we need to indicate that these rainfall estimates could, unfortunately, not be confirmed by ground measurements due

https://doi.org/10.5194/nhess-2022-83
Preprint. Discussion started: 9 March 2022


Natural Hazards and Earth System Sciences
Discussions
Open Access
EGU

653 to missing data availability (information received by the Centre National de l'Information Géo-Spatiale,
654 CNIGS, of Haiti). Fig. 8 presents the three first types of maps, while the last one is compared with the
655 first and third type in Fig. A1, in the annex. By comparing the merged satellite-gauge precipitation
656 estimate for August 2021 (Fig. 8b) with the monthly precipitation map averaged for all months of the
657 previous 20 years (Fig. 8a), we can clearly see that August 2021 was indeed marked by a higher
658 precipitation rate, which is most likely related to the Grace event. However, the most intense precipitation
659 did not affect the region hit by the 2021 earthquake but the eastern part of the peninsula, roughly covering
660 the same region as the one affected by the 2010 event (note, we did not check any landslide reactivation
661 after Grace for that area). The region hit by the 2021 earthquake was not affected by much higher monthly
662 precipitation rates than usual: for the central seismically affected zone, in the North of Les Cayes, about
663 240-280 mm had been recorded in August 2021, against a monthly average of 200 mm. Thus, just by
664 considering these data, one would not expect an important climatic contribution to slope failure
665 occurrence in the region affected by the 2021 earthquake. Still, an influence could be observed and this
666 is likely to be related to the concentration of most of the 'monthly precipitation' of August 2021 within
667 the two days (Aug. 16 and 17) of the Grace tropical storm event, just two days after the 2021 main shock.
668 As indicated above, we estimate that related precipitation has resulted in an increase of landslide surface
669 areas of about 10-15%. Due to the limited extent of zones where this check can be made (only considering
670 the cloud-free areas on the Sentinel-2 image of August 14, 2021), it was decided to map all areas covered
671 by landslides after August 14, 2021, also those which are likely to have been (re)activated by rainfall –
672 the total effect of which can barely be controlled and quantified outside the 10% of cloud-free zones
673 visible on the image collected right after the main shock. The only 'correction' that can be made is to
674 reduce the total surface area mapped as landslides by those 10-15% to estimate the one that was actually
675 affected by co-seismic slope failures: thus, instead of considering the value of 84 km^2, it is possible that
676 co-seismic landslides covered a total surface area of 'only' 75-78 km^2 – which is still three times more
677 than the total surface area covered by 2010 co-seismic landslides (close to 25 km^2).
678 To explain this great difference between the total surface areas, we will analyze the possibility of a
679 preconditioning of slope instability due to climatic events that occurred before August 2021. Therefore,
680 we compare the average monthly precipitation rates between 2000 and 2021 (Fig. 8a) with the one of
681 October 2016 (Fig. 8c). For that month, a peak of intensity of 626 mm can be observed for the area

https://doi.org/10.5194/nhess-2022-83
Preprint. Discussion started: 9 March 2022

682 between Gran Rivière De Nappe and Petite-Rivière-de-Nippes, situated immediately in the North of the
683 epicentral area of the 2021 main shock. Actually, the whole area potentially affected by the August 2021
684 earthquake had been exposed to abnormal precipitation rates of more than 400 mm in October 2016 (to
685 be considered as abnormal also when comparing with the average precipitation of all months of October
686 between 2000 and 2020, of 200-320 mm, as shown in Fig. A1). For October 2016, those values were also
687 the highest ones compared with the rest of the country; this clearly indicates that they must be related to
688 a specific climatic event, which can easily be identified as Hurricane Matthew that had crossed the
689 western peninsula (including the region hit later by the August 2021 earthquake) on October 4-5, 2016.
690 And, precisely for this region that had been exposed to abnormal precipitation rates in October 2016, we
691 could outline 324 pre-seismic landslides (yellow polygons shown above in the maps in Figs 1, 3 and 5
692 and below in Fig. 8), mapped for the period between mid-October 2016 and the end of 2017. In this
693 regard, it should be noted that we had to extend the observation period (beyond the end of 2016), as not
694 all regions were cloud-free right after the hurricane event or are still not covered by higher, 0.5-1 m,
695 resolution imagery available for that period. Outside this region, no (or only very few) clear landslide
696 activations could be identified between mid-October 2016 and the end of 2017. And, practically all 324
697 landslide zones (at least 90% of them) are located within those mapped for the August 2021 seismic event
698 (which are still marked by a much higher level of denudation compared to the October 2016 activation).
699 These observations allow us to conclude that the Hurricane Matthew event has preconditioned slope
700 instability over the region hit later by the August 2021 earthquake. This preconditioning factor could also
701 explain why three times larger surface areas have been affected by landslides in 2021 compared with
702 2010. Further, it must be added that the 2010 earthquake had not been preceded by any particular
703 hurricane event during the previous ten years, at least not by any storm that had caused abnormal
704 precipitation amounts specifically within the region hit by the 2010 earthquake. However, in the
705 discussion, we will also consider a general influence of tropical storms on the distribution of the
706 landslides triggered in 2010 (and also for those triggered in 2021, in addition to the Hurricane Matthew
707 effect), notably to explain why numerous landslides had occurred very far from the seismic source zone.

https://doi.org/10.5194/nhess-2022-83
Preprint. Discussion started: 9 March 2022

Natural Hazards and Earth System Sciences
Discussions

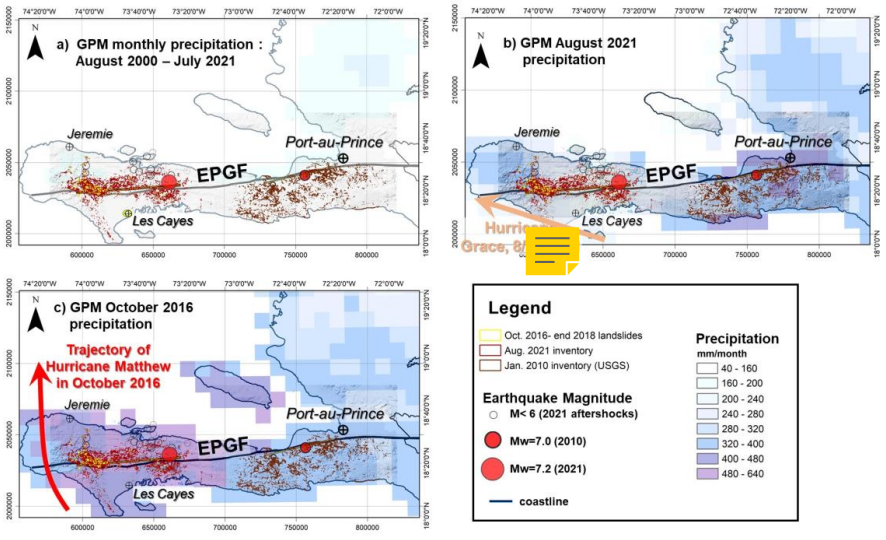

Figure 8: Monthly Global Precipitation Measurement Mission (NASA) maps (0.1° resolution, values in mm/month) for southwestern Haiti, (a) for all months between August 2000 and July 2021, (b) for August 2021 (with indication of the track of Hurricane Grace – at that stage still to be considered as a tropical storm), and (c) for October 2016 (marked by the Hurricane Matthew event).

3.4 Shaking intensity maps

Above, we fist analyzed the possible climatic influence on seismically induced slope failures as it could affect the landslide distribution and thus has to be taken into consideration when assessing and interpreting the seismic effect on landslide occurrence. The latter will only be analyzed here at regional scale. Therefore, we compare the landslide distributions observed for the 2010 and 2021 events with the respective estimated Arias Intensity (Ia) attenuation maps, computed by applying Eq. (7b) introduced above, as recommended by Wilson and Keefer (1985) and also by later studies (e.g., Harp and Wilson, 1995, among many others). The map in Fig. 9a presents the 2010 and 2021 mainshock Ia attenuation values, with a maximum shaking intensity of 11.2 m/s computed for the 2021 event and 7.9 m/s for 2010 (respective maps are partly overlapping in the central region, but not summed up, keeping the individual values). This map shows that all 2010 and 2021 landslides are included within a zone marked by an Ia

https://doi.org/10.5194/nhess-2022-83
Preprint. Discussion started: 9 March 2022

threshold of 0.2 m/s (close to the one proposed by Keefer and Wilson, 1989, for disrupted slides and falls). Actually, for 2021, 99% of the total landslide surface areas are even located within a zone marked by Ia values lager than 1 m/s; however, only 80% of the total surface areas of the 2010 landslides are included within the respective Ia >= 1 m/s zone. Thus, the latter mass movements appear as more 'dispersed' with respect to the estimated seismic intensity attenuation than the 2021 ones. Notwithstanding this dispersion, and the overlap of Ia values larger than 0.2 m/s in the central zone between the two blind fault ruptures of 2010 and 2021, not a single landslide of 2010 seems to have been reactivated in 2021. This observation raises the question if the central 'landslide gap' is due to an overestimation of the Ia values in this central zone (as this zone is marked by Ia values above the aforementioned minimum threshold of 0.2 m/s, for both events, and thus should have been affected by landslides both in 2010 and 2021, according to the shaking intensity prediction parameter), or if this zone is simply less susceptible to (seismic) slope failures.

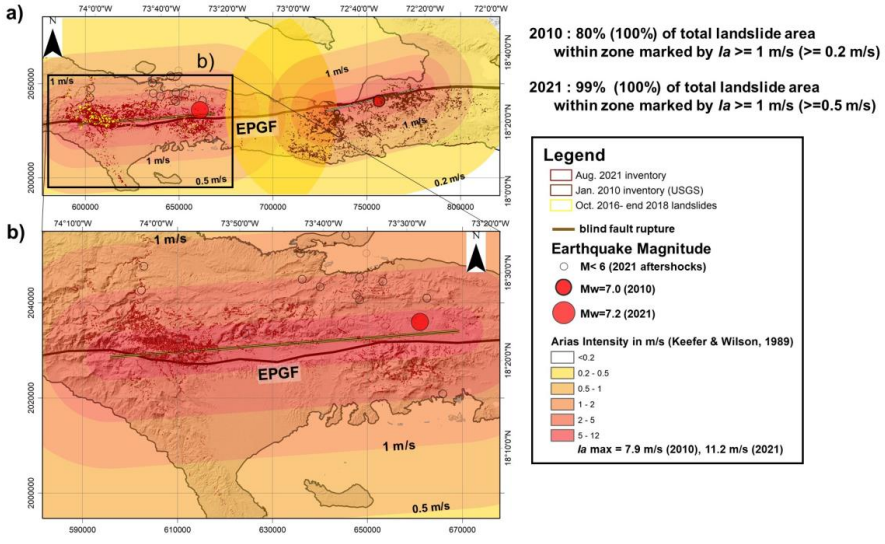

Figure 9: a) Arias Intensity (Ia) attenuation maps computed (by using Eq. 7b, by Keefer and Wilson, 1989) for the 2010 and 2021 main shocks in Haiti; see also indication of % of total surface area of landslides observed for different Ia thresholds. b) Focus on the respective map computed for the 2021 event.

https://doi.org/10.5194/nhess-2022-83
Preprint. Discussion started: 9 March 2022


Natural Hazards and Earth System Sciences
Discussions

742 To answer this and other related questions, a full landslide susceptibility analysis has been completed
743 and will be presented in another paper. Here, only the possible links between landslide distribution the
744 aforementioned seismotectonic and climatic factors will be discussed.

745 4 Discussion

746 From the comparison of the two landslide catalogues (2010 and 2021), we could infer that apparently
747 not a single landslide triggered in August 2021 occurred within the zone previously impacted by the 2010
748 event. There is a gap of about 10 km between the westernmost 2010 and the easternmost 2021 landslide
749 (see gap between the general outlines of the maximum extent of landslides triggered in 2010 and in 2021
750 shown on the map in Fig. 5a). Thus, we assume that there was no obvious preconditioning of landslide
751 generation in 2021 by the 2010 event, while landslide studies completed in other parts of the World (e.g.,
752 by Parker et al., 2015, for events in New Zealand) could outline an influence of previous earthquakes on
753 landslide occurrence during later events. The absence of this influence by the 2010 earthquake is
754 probably due to the long distance (the 'gap') of about 60 km between the fault segments that ruptured in
755 2010 and in 2021. However, by citing Saint Fleur et al. (2020), Stein et al. (2021) hint at an older event,
756 of 1770, with an assumed magnitude of 7.5 and an epicenter located precisely in the gap between the
757 2010 and 2021 blind fault ruptures, which could also have affected the region hit by the 2021 earthquake.
758 At present, we cannot exclude that this older event had preconditioned some slopes (by soil weakening,
759 rock fracturing) affected by some larger landslides in 2021; however, very shallow slope failures initiated
760 in 1770 are unlikely to have stayed in place over such a long period of more than 250 years, as they
761 would have been 'washed' away by the next tropical rains.
762 Second, none of the two earthquakes triggered very massive landslides, such as deep-seated rockslides
763 with a volume of more than 20 10^6 m^3 (while extensive areas are covered by layered and weathered
764 limestone that could also produce massive slope failures; the related geological influence on landslide
765 occurrence will be analyzed in the landslide susceptibility paper presently under preparation). Such
766 massive failures have been observed after many M7+ events in other mountainous regions of the world:
767 see Fan et al. (2018) for the 2008 Mw=7.9 earthquake in China, or Havenith et al. (2015) for a series of
768 M>7 events that hit Central Asian mountain regions during the last 120 years. This is partly due to the

https://doi.org/10.5194/nhess-2022-83
Preprint. Discussion started: 9 March 2022

769 fact that the regions hit by the two earthquakes in Haiti are covered by mountains of limited elevation
770 changes, typically less than 1000 m – while, for instance, the Longmenshan Mountains hit by the 2008
771 Wenchuan earthquake, present elevation changes of up to 3000 m over relatively short (<6 km) distances
772 (Fan et al., 2018). This fact, combined with the higher magnitude of the Wenchuan earthquake (Mw=7.9),
773 could partly explain the much larger number of massive rockslides triggered by the latter event in China.
774 As third general observation, we highlight the fact that the 2010 event triggered most landslides in the
775 South of the activated fault segment, while in August 2021 about 2/3 of all landslides were triggered in
776 the North of it, within the hanging wall (according to the fault mechanism provided by the USGS
777 Earthquake Hazard Program page, earthquake.usgs.gov). In this regard, the Wenchuan earthquake has
778 clearly marked the effect of the hanging wall on the landslide distribution: about 90 % of all landslides
779 were triggered on top of the reverse fault dipping towards the West-Northwest, only a minor portion
780 occurred on the more 'stable' foot wall (Gorum et al., 2011; Fan et al., 2018). The 'hanging wall effect'
781 on landslide triggering can be explained by stronger upward oriented shaking that contributes to a higher
782 surface acceleration and more intense slope failures; additionally, all (or most of the) aftershocks
783 occurred within the hanging wall, increasing the seismic shaking intensity cumulated over the active
784 seismic period in the related surface area, which could have contributed to prolongated landslide activity
785 as well (to be added to the climatic effect introduced above and discussed below). This effect may thus
786 also be at the origin of the more widespread landslide occurrence in the North of the 2021 blind fault
787 rupture. The reduced number of landslides induced on the hanging wall side of the 2010 fault rupture can
788 be explained by the absence of high and steep slopes (onshore) on this side. Actually, a few known
789 massive landslides occurred near the coast, but are mostly located on submarine slopes in the 2010
790 hanging wall zone. Three of them reportedly also caused Tsunami waves (see Olson et al., 2011, among
791 others) – a phenomenon that was not observed for the 2021 event, as the coasts are located farther away
792 from the seismic source zone.
793 In section 2, we have outlined the two different types of landslide mapping techniques applied to the
794 2010 event (by Harp et al., 2016) and to the August 14, 2021, earthquake (the new inventory presented
795 here). Our somewhat 'rougher' mapping technique adapted to the lower resolution imagery immediately
796 available right after the 2021 earthquake first explains the much smaller number of landslides (7091)
797 mapped around the fault segment that ruptured in 2021, compared to the 2010 event (>23,000 landslides

https://doi.org/10.5194/nhess-2022-83
Preprint. Discussion started: 9 March 2022


Natural Hazards and Earth System Sciences
Discussions

mapped by Harp et al., 2016). Second, we acknowledge that the mapping of coherent landslide zones compared with the outlining of individual landslide sources and flows by Harp et al. (2016) can result in 'over-mapping' of large landslides and, thus, in decreasing the weight of of the smaller ones, which also affects size-frequency statistics. Additionally, it is likely that thousands of smaller landslides could not be mapped from the medium-resolution Sentinel-2 imagery (10 m) and the higher resolution imagery (0.5 – 1 m) available on GEPro for 50% of the target area before the end of 2021. To refine our landslide mapping in future, higher resolution imagery must be used for the whole area affected by the 2021 event, and automatic landslide identification techniques shall be applied by combining image analysis and machine learning as proposed by Amatya et al. (2021). Actually, the 'manual' mapping applied now would take too much time to outline the many thousands of very small landslides that have not been identified so far. Those would contribute to the increase of the weight of the smaller landslides in the 2021 inventory, especially of those smaller than 2000 m^2.

From the preceding we can infer that the mapping of additional smaller landslides will not really modify the power-law decay part presented in Fig. 7 (for which also the 2021 catalogue can be considered as complete), and increase the absolute value of the related decay exponent – which is smaller (2.0-2.1) than the one proposed by Malamud et al. (2004) as 'universal' value (2.4) for landslide events. Interestingly, the same graph in Fig. 7 shows that the exponent of the power-law decay part of the 2010 landslide frequency-density distribution is even higher (2.6) than the value proposed by Malamud et al. (2004). One reason for the different values could be that the decay exponent value of -2.4 is simply not as universal as suggested by Malamud et al. (2004), a hypothesis that is supported by the findings of Van den Eeckhaut et al. (2007), Stark and Guzzetti (2009) and Tanyas et al. (2019) who also reported varying exponent values (that are still close to the one of -2.4, typically between -1.8 and -2.8). Especially, the higher value obtained for the Harp et al. (2016) inventory indicates that this value could be influenced by the mapping technique (also related to the availability of high-resolution imagery, and to the outlining of coherent landslides vs distinguishing between individual landslide zones within a larger mass movement).

Another reason for the smaller number of landslides mapped for the 2021 event (that does not exclude the first one) would be related to the fact that the landslides triggered in 2010 mainly consisted of narrow slides and flows in weathered limestone rocks. Thus, the type of rock affected could have an influence

https://doi.org/10.5194/nhess-2022-83
Preprint. Discussion started: 9 March 2022


Natural Hazards and Earth System Sciences
Discussions

827 on the power-law decay of landslide size-frequency distributions. For instance, Havenith et al. (2015)
828 showed for the Tien Shan Mountains that the landslide distribution in soft soils are marked by a higher
829 decay exponent (~2.1) than the one in hard rocks (exponent of -1.9 for mass movements in areas mainly
830 made of magmatic or sedimentary hard rocks). Anyway, in order to be able to exclude any artificial effect
831 on the size-frequency statistics, the new 2021 landslide event catalogue has to be revised once all the
832 area is covered by higher resolution imagery (at least <= 1 m pixel size). After this work, we may then
833 also provide a more definite answer to the related questions: first, is the new 'complete' inventory for
834 2021 characterized by the same power-law decay exponent as the present one (= - 2) or do we obtain a
835 new one closer to the value (= -2.4) proposed by Malamud et al. (2004)? Second, shall we observe the
836 rollover for a landslide class of about 300 m^2, or for a different class, or for none (at least not above 100
837 m^2), just as it seems to be the case for the 2010 landslide inventory by Harp et al. (2016)? If all parameter
838 values will be close to those predicted by the equations by Malamud et al. (2004), then, the future 2021
839 inventory should contain close to 100,000 landslide polygons, according to the graph shown in Fig. 7 –
840 which seems to be an unrealistically high number, even if that inventory will be refined as proposed
841 above. If, however, a rollover is observed for a landslide class of about 300 m^2 (now it appears for a
842 much larger class of about 3000 m^2) as proposed by Malamud et al. (2004), but the power-law decay is
843 marked by a lower absolute value of the exponent (closer to present one, near -2.1), then, the new
844 inventory should contain about 20,000 landslides (closer to the number predicted by Havenith et al., 2016
845 for such an event) according to the graphical prediction in Fig. 7. Certainly, there is also the possibility
846 that none of the predictions proposed by Malamud et al. (2004) would be verified after landslide
847 remapping on the basis of higher resolution imagery and applying automatic landslide detection
848 techniques – and then no estimate of the number of landslides contained in the future inventory can be
849 provided right now. Among the three possibilities, we think that option 2, combining a rollover for a
850 landslide surface area of 300 m^2 with a lower absolute power-law decay component (~2.1) shall be the
851 most realistic one marking a complete 2021 landslide inventory. This assessment is based on our present
852 mapping experience. Also, the total number of landslides of 20,000, predicted by the frequency-density
853 curves proposed by Malamud et al. (2004) for those values (see graph in Fig. 7), would be of the same
854 order of magnitude as the number predicted by Havenith et al. (2016) for such a Mw=7.2 earthquake and
855 the observed background conditions (~13,500).

https://doi.org/10.5194/nhess-2022-83
Preprint. Discussion started: 9 March 2022

Disregarding the likely influence of the inventory completeness on the different size-frequency statistics of the two landslides inventories related to the 2010 and 2021 events, the changing climatic conditions could also affect those statistics. Notably, it could be shown that the climatic contribution to landslide activity in 2021 might be twofold: first, some post-seismic intensification of slope failures could be observed after the tropical storm Grace event that had crossed the earthquake region on August 16-17, two days after the main shock. However, related effects cannot really be quantified as only 10% of the total surface area potentially affected by the earthquake appeared as cloud-free on imagery available right after the August 14 main shock and before August 16 (Grace event). For those limited areas, we estimate that storm Grace caused additional 10-15 % of slope failures with respect to the purely earthquake-induced landslide activation. Second, by comparing the 2016-2017 landslide distribution with the one observed after August 14, 2021, it can be seen that most of the October 2016 – end 2017 landslides occurred within the same region as the 2021 ones and most were clearly reactivated by the seismic shaking in August 2021 (while also many of them had been revegetated in between). Above we could show that Hurricane Matthew had crossed the western part of the peninsula in October 2016, producing an abnormal amount of precipitation precisely over the area recently hit by the earthquake (see GPM maps in Fig. 8), and where also numerous landslides had occurred just after mid-October 2016. Therefore, it is very likely that this climatic event has triggered many of the pre-seismic (pre-2021 and even pre-2018) landslides, which preconditioned slope instability all over the area hit by the 2021 earthquake. The double hurricane effect (by Matthew in 2016 and by Grace just after the 2021 main shock) observed in the area hit by 2021 earthquake could be responsible for the proportionally larger size of the 2021 landslides (preconditioning of slope failures and post-seismic intensification) compared to the 2010 ones, and thus explain the lower absolute value of the power-law decay. As indicated above for other aspects, the related conclusion still requires some remapping of the 2021 landslides and ‘finetuning’ of their outlines.

Additionally, the combined seismic and climatic influence could also explain the very different spatial landslide distribution characteristics of the 2010 and 2021 catalogues: the relative dispersion of landslides observed after the 2010 event could thus be partly related to the spatially highly variable effect of tropical storms and hurricanes on landslide activity (acting over a longer period, with an influence that could last over tens of years), partly overprinting the more concentrated seismic effect (resulting in

https://doi.org/10.5194/nhess-2022-83
Preprint. Discussion started: 9 March 2022


Natural Hazards and Earth System Sciences
Discussions

clusters of mass movements near the seismic source zone). The same dispersion might also have been observed for the 2021 event if the central part of the seismically affected area had not been hit by that major climatic event just five years before – doubling the landslide concentration effect in that area (specifically for this event). However, we acknowledge that a quantification of these opposite effects of climatic events, both on landslide dispersion and on their concentration, requires a more detailed analysis, also focusing on specific sites, by completing numerical simulations of mass movements affected by variable climatic (modelling changing groundwater level) and seismic influences (including the effect of rock structures and types of lithologies and morphologies on shaking polarization and amplification). A related landslide spatial distribution analysis should then also consider the influence of extensive deforestation on slope destabilization, all over the country of Haiti. Actually, deforestation is responsible for the decrease of 90% of the primary forest over the last few tens of years, especially in the southern regions of Haiti where the two earthquake events had occurred (see Hedges et al., 2018). As mostly shallow landslides occurred in 2010 and 2021, the effect of deforestation on the destabilization of shallow soils and weathered rock cover must be taken into consideration for landslide occurrence prediction. Such an extensive study would thus require the creation of an integrated seismotectonic-morpho-geological-climatic-soil cover model allowing us to fully understand changing landslide activity in Haiti – which is not the target of the present analysis.

As for the climatic part, here, we only present regional data to outline some general seismic influences on landslide activity induced by the 2010 and 2021 earthquakes. Related maps (Fig. 9) show that the aforementioned gap of landslides between the areas affected by the earthquakes in 2010 and 2021 would indeed be marked both by a lower shaking intensity (but showing values that are still larger than the threshold Ia values observed elsewhere for landslide occurrence) and lower landslide susceptibility (still to be published).

5 Conclusions

In this paper we first presented the new landslide inventory created for the Mw=7.2 Nippes earthquake that occurred on August 14, 2021, in Haiti. Related spatial and statistical characteristics have been compared with those of the landslides mapped by others for the previous, Mw=7.0, January 12 (2010),

https://doi.org/10.5194/nhess-2022-83
Preprint. Discussion started: 9 March 2022


Natural Hazards and Earth System Sciences
Discussions

912 earthquake that had occurred along the same fault zone (EPGF zone) but more to the East. Considering
913 a series of uncertainties affecting the landslide statistics (related to the mapping technique, including the
914 uncertain number of particularly small landslides triggered in 2021) and the environmental information
915 (including the climatic and geological conditions), this comparison allowed us to highlight the following
916 points: 1) the 2021 earthquake triggered landslides over wider surface areas than the one in 2010; 2) size-
917 frequency statistics computed for the two landslide catalogues present a clear power-law decay, marked
918 by different exponent values; however, a rollover is only observed for the 2021 inventory (but for a
919 relatively large landslide area class, hinting at an incompleteness of the inventory, for the smaller
920 landslides); for the 2010 data such feature does not appear, at least not for landslide sizes above 100 m^2,
921 hinting at an 'over-completeness' of that inventory (compared with others published); 3) climatic
922 preconditioning of slope instability could be 'proved' for the 2021 event, mainly in connection with the
923 impacts of recent hurricanes in the 2021 affected region, which could also partly explain the more
924 extensive landslide activity observed in 2021; 4) the 2010 landslides seem to be more dispersed around
925 the epicentral area than the 2021 slope failures, which could be due to the opposite climatic effect
926 inducing spatially more variable slope destabilization (also as no particular storm had hit the 2010
927 affected region just before or after the seismic event, as it was the case in 2021); this dispersion effect
928 can also be enhanced by the spatially varying deforestation that is locally very intense in the target areas.
929 We estimate that this proof of a combined seismic and climatic influence on landslide activity (possibly
930 augmented by morpho-geological and soil cover effects not studied in detail here) opens new avenues
931 for geohazard research, especially for regions like Haiti that are regularly hit both by severe earthquakes
932 and weather events. We also think that preconditioning of slope failures by multiple events over longer
933 terms, including by former earthquakes, should be studied more in detail as this preconditioning could
934 highly contribute both to regional and local landslide hazards over short and longer terms. A full analysis
935 of such a scenario would require the development of an integrated seismotectonic-morpho-geological-
936 climatic-soil (and vegetation) cover model, which can only be completed through an extensive
937 international multi-disciplinary collaboration around this target – which is obviously missing for Haiti.
938 Assessment of related risk would further require the involvement of experts in social geography and
939 economy. Only when this goal is achieved, we could really work on the prevention of at least parts of
940 another future earthquake disaster in Haiti.

https://doi.org/10.5194/nhess-2022-83
Preprint. Discussion started: 9 March 2022

Natural Hazards and Earth System Sciences
Discussions

Acknowledgments

This study was partly supported by the 'Earthquake Hazard and Vulnerability assessment – developing innovative solutions for sustainable Risk Reduction and Communication in Haiti' project funding (2019-2024) provided by the Belgian ARES – ACADÉMIE DE RECHERCHE ET D'ENSEIGNEMENT SUPÉRIEUR.

References

Acker, G. and Leptoukh, G.: Online Analysis Enhances Use of NASA Earth Science Data, Eos, Trans. AGU, 88(2), 14–17, 2007.

Amatya, P., Kirschbaum, D., Stanley, T., and Tanyas, H.: Landslide mapping using object-based image analysis and open source tools, Eng. Geol., 282, 10 p., doi:10.1016/j.enggeo.2021.106000, 2021.

Arias, A.: A measure of earthquake intensity, In Seismic design for Nuclear Powerplants, R.J. Hansen (ed), MIT Press, Cambridge, Massachusetts, 438–483, 1970.

Calais, E., Freed, A., Mattioli, G., Amelung, F., Jónsson, S., Jansma, P., Hong, S. H., Dixon, T., Prépetit, C., and Momplaisir, R.: Transpressional rupture of an unmapped fault during the 2010 Haiti earthquake, Nature Geoscience, 3(11), 794–799, doi:10.1038/ngeo992, 2010.

Fan, X., Juang, C.H., Wasowski, J., Huang, R., Xu, Q., Scaringi, G., van Westen, C.J., and Havenith, H.B.: What we have learned from the 2008 Wenchuan Earthquake and its aftermath: A decade of research and challenges, Eng. Geol., 241, 25–32, doi:10.1016/j.enggeo.2018.05.004, 2018.

Frankel, A., Harmsen, S., Mueller, C., Calais, E., and Haase, J.: Seismic hazard maps for Haiti. Earthquake Spectra, 27(SUPPL. 1), 23–41. doi:10.1193/1.3631016, 2011.

Fritz, H. M., Hillaire, J. V., Molière, E., Wei, Y., and Mohammed, F.: Twin tsunamis triggered by the 12 January 2010 Haiti earthquake, Pure and Applied Geophysics, 170(9), 1463–1474, doi:10.1007/S00024-012-0479-3, 2013.

https://doi.org/10.5194/nhess-2022-83
Preprint. Discussion started: 9 March 2022

967 Gorum, T., Fan, X., van Westen, C.J., Huang, R., Xu, Q., Tang, C., and Wang, G.: Distribution pattern
968 of earthquake-induced landslides triggered by the 12 May 2008 Wenchuan earthquake, Geomorph.,
969 133(3–4), 152–167, doi:10.1016/j.geomorph.2010.12.030, 2011.
970 Gorum, T., van Westen, C.J., Korup, O., van der Meijde, M., Fan, X., and van der Meer, F.D.: Complex
971 rupture mechanism and topography control symmetry of mass - wasting pattern, 2010 Haiti earthquake,
972 Geomorph., 184, 127–138, doi:10.1016/j.geomorph.2012.11.027, 2013.
973 Harp, E.L. and Wilson, R.C.: Shaking intensity thresholds for rock falls and slides : evidence from 1987
974 Whittier Narrows and Superstition Hills earthquake strong-motion records, Bull. Seis. Soc. Am., 85,
975 1739–1757, 1995.
976 Harp, E.L., Jibson, R.W., and Schmitt, R.G.: Map of landslides triggered by the January 12, 2010, Haiti
977 earthquake: U.S. Geological Survey Scientific Investigations Map 3353, 15 p., 1 sheet, scale 1:150,000.
978 doi:10.3133/sim3353, 2016.
979 Havenith, H. B., Jongmans., D., Faccioli., E., Abdrakhmatov., K., and Bard, P.Y.: Site effect analysis
980 around the seismically induced Ananevo rockslide, Kyrgyzstan, Bull. Seis. Soc. Am., 92(8), 3190–3209,
981 2002.
982 Havenith, H.-B., Strom, A., Caceres, F., and Pirard, E.: Analysis of Landslide Susceptibility in the
983 Suusamyr Region, Tien Shan: Statistical and Geotechnical Approach, Landslides, 3, 39–50,
984 doi:10.1007/s10346-005-0005-0, 2006.
985 Havenith, H.B., Strom, A., Torgoev, I., Torgoev, A., Lamair, L., Ischuk, A., Abdrakhmatov, K.: Tien Shan
986 Geohazards Database: Earthquakes and Landslides, Geomorph., 249, 16–31,
987 doi:10.1016/j.geomorph.2015.01.037, 2015.
988 Hedges, S.B., Cohen, W.B., Timyan, J., and Yang, Z.: Haiti's biodiversity threatened by nearly complete
989 loss of primary forest, Proc. Nat. Ac. Sc., 115(46), 11850–11855, doi: 10.1073/pnas.1809753115, 2018.
990 Keefer, D.K. and Wilson, R.C.: Predicting earthquake-induced landslides, with emphasis on arid and
991 semi-arid environments, In Landslides in a Semi-arid environment (Inland Geological Society, Sadler
992 and Morton, eds.), 2, 118–149, 1989.
993 Martinez, S.N., Allstadt, K.E., Slaughter, S.L., Schmitt, R., Collins, E., Schaefer, L.N., and Ellison, S.:
994 Landslides triggered by the August 14, 2021, magnitude 7.2 Nippes, Haiti, earthquake, U.S. Geological
995 Survey Open-File Report 2021–1112, 17 p., doi:10.3133/ ofr20211112, 2021.

https://doi.org/10.5194/nhess-2022-83
Preprint. Discussion started: 9 March 2022

996 Meunier, P., Hovius, N., and Haines, J. A.: Topographic site effects and the location of earthquake
997 induced landslides, Earth and Planetary Science Letters, 275(3-4), 221–232,
998 doi:10.1016/j.epsl.2008.07.020, 2008.
999 Okuwaki, R. and Fan, W.: Oblique convergence causes both thrust and strike-slip ruptures during the
1000 2021 M 7.2 Haiti earthquake, Geoph. Res. Letters, 49(2), 12 p., doi:10.1029/2021GL096373, 2022.
1001 Olson, S., Green, R., Lasley, S., Martin, N., Cox, B., Rathje, E., Bachhuber, J., and French, J.:
1002 Documenting Liquefaction and Lateral Spreading Triggered by the 12 January 2010 Haiti Earthquake,
1003 Earthquake Spectra, 27, 93–116, doi:10.1193/1.3639270, 2011.
1004 Parker, R.N., Hancox, G.T., Petley, D.N., Massey, C.I., Densmore, A.L., and Rosser, N.J.: Spatial
1005 distributions of earthquake-induced landslides and hillslope preconditioning in the northwest South
1006 Island, New Zealand, Earth Surface Dynamics, 3 (4), 501–525, doi:10.5194/esurf-3-501-2015, 2015.
1007 Petley, D.: Landslides from the 14 August 2021 earthquake in Haiti, On
1008 blogs.agu.org/landslideblog/2021/09/03/landslides-from-the-14-august-2021-earthquake-in-haiti, 2021.
1009 Poupardin, A., Calais, E., Heinrich, P., Hébert, H., Rodriguez, M., Leroy, S., Aochi, H., and Douilly, R.:
1010 Deep submarine landslide contribution to the 2010 Haiti earthquake tsunami, Nat. Hazards Earth Syst.
1011 Sci., 20, 2055–2065, doi:10.5194/nhess-20-2055-2020, 2020.
1012 Saint Fleur, N., Klinger, Y., and Feuillet, N.: Detailed map, displacement, paleoseismology, and
1013 segmentation of the Enriquillo-Plantain Garden Fault in Haiti, Tectonophysics, 778, 25 p.,
1014 doi:10.1016/j.tecto.2020.228368, 2020.
1015 Sassa, S. and Takagawa, T.: Liquefied gravity flow-induced tsunami: first evidence and comparison
1016 from the 2018 Indonesia Sulawesi earthquake and tsunami disasters, Landslides, 16, 195–200.
1017 doi:10.1007/s10346-018-1114-x, 2018.
1018 Stark, C.P. and Guzzetti, F.: Landslide rupture and the probability distribution of mobilized debris
1019 volumes, J. Geoph. Res.: Earth Surface, 1–16, doi:10.1029/2008JF001008, 2009.
1020 Stark, C. P. and Hovius, N.: The characterization of landslide size distributions, Geoph. Res. Letters,
1021 28(6), 1091–1094, doi:10.1029/2000GL008527, 2001.
1022 Stein, R.S., Toda, S., Lin, J., and Sevilgen, V.: Are the 2021 and 2010 Haiti earthquakes part of a
1023 progressive sequence? Temblor, doi:10.32858/temblor.197, 2021.
1024 Symithe, S. J., Calais, E., Haase, J. S., Freed, A. M., and Douilly, R.: Coseismic Slip Distribution of the

https://doi.org/10.5194/nhess-2022-83
Preprint. Discussion started: 9 March 2022

2010 M 7.0 Haiti Earthquake and Resulting Stress Changes on Regional Faults, Bull. Seis. Soc. Am., 103, 2326–2343, doi:10.1785/0120120306, 2013.

Tanyas, H., van Westen, C.J., Allstadt, K.E., and Jibson, R.W.: Factors controlling landslide frequency–area distributions, Earth Surf. Process. Land. (44), 900–917, doi:10.1002/esp.4543, 2019.

Terrier, M., Bialkowski, A., Nachbaur, A., Prépetit, C., and Joseph, Y. F.: Revision of the geological context of the Port-au-Prince metropolitan area, Haiti: implications for slope failures and seismic hazard assessment, Nat. Hazards Earth Syst. Sci., 14, 2577–2587, doi:10.5194/nhess-14-2577-2014, 2014.

Ulysse, S., Boisson D., Prépetit, C., and Havenith, H.-B.: Site Effect Assessment of the Gros-Morne Hill Area in Port-au-Prince, Haiti, Part A: Geophysical-Seismological Survey Results, Geosciences, 8(4), 142, 1-22. doi:10.3390/geosciences8040142, 2018.

Van Den Eeckhaut, M., Poesen, J., Govers, G., Verstraeten, G., and Demoulin, A.: Characteristics of the size distribution of recent and historical landslides in a populated hilly region, Earth and Planetary Science Letters, 256(3), 588–603, doi:10.1016/j.epsl.2007.01.040, 2007.

Wilson, R.C. and Keefer, D.K.: Predicting the areal limits of earthquake-induced landsliding, In Evaluating Earthquake Hazards in the Los Angeles Region - An Earth Science Perspective (Ziony , ed.), U.S. Geol. Surv. Prof. Paper 1360, 316-345, 1985.

Xu, C., Shyu, J. B. H., and Xu, X.: Landslides triggered by the 12 January 2010 Port-au-Prince, Haiti, Mw = 7.0 earthquake: visual interpretation, inventory compiling, and spatial distribution statistical analysis, Nat. Haz. Earth Syst. Sci., 14(7), 1789–1818, doi:10.5194/nhess-14-1789-2014, 2014.

https://doi.org/10.5194/nhess-2022-83
Preprint. Discussion started: 9 March 2022

Natural Hazards and Earth System Sciences
Discussions

1051 **Annex**

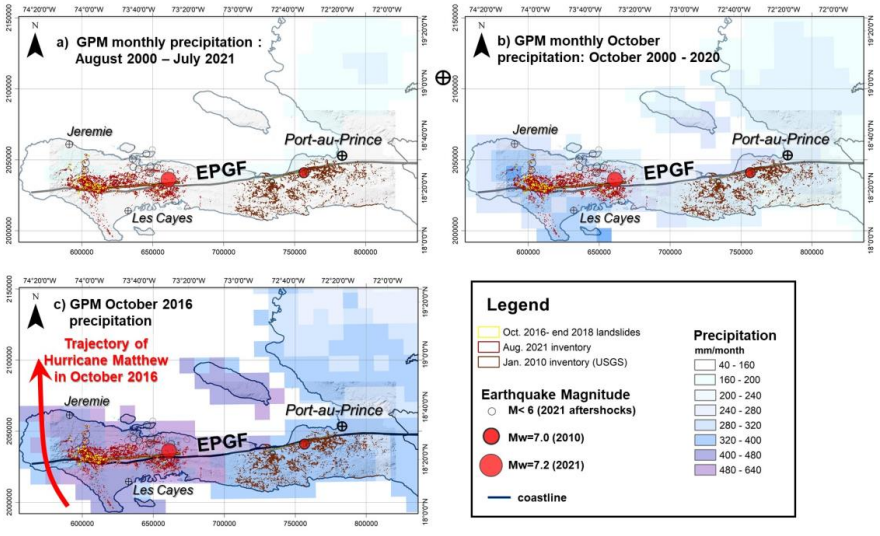

1052

1053 **Figure A1: Monthly Global Precipitation Measurement Mission (NASA) maps (0.1° resolution, values in**
1054 **mm/month) for southwestern Haiti, (a) for all months between August 2000 and July 2021, (b) for the month**
1055 **of October between 2000 and 2020, and (c) for October 2016 (marked by the Hurricane Matthew event).**